Tensile Behavior of FFF PLA: Experimental Characterization and Numerical Simulation

Maria Eduarda Bordignon Enriconi
a62878

Bragança, Portugal

July 2025

Tensile Behavior of FFF PLA: Experimental Characterization and Numerical Simulation

Maria Eduarda Bordignon Enriconi
a62878

Dissertation presented to **Escola Superior de Tecnologia e Gestão de Bragança** in a double degree program with **Universidade Tecnológica Federal do Paraná – Campus Curitiba** to obtain the Master of Science Degree in Mechanical Engineering.

Supervised by:

Professor Dr. João Eduardo P. C. Ribeiro
Professor Dr. João da Rocha e Silva
Professora Márcia de Araujo

Bragança, Portugal

July 2025

Acknowledgements

I am deeply grateful to everyone who walked this journey with me.

To my fiancé, Fernando – thank you for your strength, patience, and constant belief in me. I couldn't have done this without you.

To my family – thank you for always believing in me and supporting my choices, no matter the distance.

To Tuca, Pedro, Senai, and Junior – thank you for being part of this journey, even from afar. University life simply wasn’t the same without you.

To Bia, Nelson, and Caio – thank you for being my Bragança family. Your friendship brought warmth, laughter, and unforgettable memories to this journey.

I am also grateful to my professors, whose guidance and generosity of knowledge shaped both my academic and personal development. To UTFPR and IPB, thank you for the opportunity to learn, explore, and evolve in two academic environments that have enriched me deeply.

Finally, I gratefully acknowledge the support of the project “0049_NATUR_FAB_2_E – Fomento de la especialización inteligente, transición industrial y emprendimiento a través de nuevos materiales basados en recursos endógenos compatibles con tecnologías de fabricación aditiva de gran formato,” funded through the Programme Interreg VI A España–Portugal (POCTEP), whose contribution was essential to the realization of this research.

Resumo

A Fabricação por Filamento Fundido (FFF) é um método amplamente utilizado de manufatura aditiva, conhecido por sua eficiência no uso de materiais e versatilidade geométrica. No entanto, o desempenho mecânico das peças impressas por FFF é influenciado pela variabilidade do processo, especialmente em polímeros frágeis como o ácido polilático (PLA). Esta dissertação combina uma revisão de abordagens de simulação numérica com um estudo experimental-numérico para estabelecer uma metodologia de avaliação mecânica confiável para peças de PLA impressas por FFF. A revisão categoriza os modelos existentes com base no escoamento do material fundido, comportamento térmico e simulação estrutural, destacando limitações na integração multifísica e na validação experimental. Experimentalmente, foram realizados ensaios de tração utilizando Extensômetro de Vídeo Digital (DVE) e Correlação de Imagens Digitais bidimensional (2D-DIC), revelando desafios relacionados à fratura prematura, defeitos entre camadas e mapeamento de deformações. Um modelo de elementos finitos foi desenvolvido para simular o comportamento elástico em condições padronizadas, apresentando concordância com o ensaio mais representativo. Os resultados apoiam o desenvolvimento de procedimentos de metodologias de ensaios padronizados e de referenciais para simulação, contribuindo para os objetivos do projeto NaturFAB no avanço de trabalho sustentáveis e com origem local para manufatura aditiva.

Palavras-chave: Fabricação por Filamento Fundido (FFF); Ácido Polilático (PLA); Extensômetro de Vídeo Digital (DVE); Correlação de Imagens Digitais (DIC); Análise por Elementos Finitos (FEA).

Abstract

Fused Filament Fabrication (FFF) is a widely adopted additive manufacturing method known for its material efficiency and geometric versatility. However, the mechanical performance of FFF-printed parts is highly affected by process-dependent variability, particularly in brittle polymers such as polylactic acid (PLA). This thesis combines a critical review of numerical simulation approaches with an experimental–numerical study to establish a methodology for reliable mechanical evaluation of FFF-printed PLA. The review categorizes existing models based on melt flow, thermal behavior, and structural simulation, highlighting limitations in multiphysics coupling and experimental validation. Experimentally, tensile tests were performed using Digital Video Extensometer (DVE) and Digital Image Correlation (2D-DIC), revealing challenges related to premature fracture, interlayer defects, and strain acquisition. A finite element model was developed to simulate the elastic behavior under standardized conditions, showing strong agreement with the most representative test. The findings support the development of repeatable test procedures and simulation benchmarks, contributing to the goals of the NaturFAB project in advancing sustainable and locally sourced additive manufacturing workflows.

Keywords: Fused Filament Fabrication (FFF); Polylactic Acid (PLA); Digital Video Extensometer (DVE); Digital Image Correlation (DIC); Finite Element Analysis (FEA).

Index

List of Figures

List of Tables

Abbreviations

ABS	Acrylonitrile Butadiene Styrene
AFM	Atomic Force Microscopy
AI	Artificial Intelligence
AM	Additive Manufacturing
ANN	Artificial Neural Network
APS-C	Advanced Photo System type-C
BAAM	Big Area Additive Manufacturing
CAD	Computer-Aided Design
CF	Carbon Fiber
CFD	Computational Fluid Dynamics
CFF	Continuous Fiber Filament
CFRC	Continuous Fiber-Reinforced Composite
CM	Computational Model
CMM	Coordinate Measuring Machine
CS	Cooling and Solidification
CV%	Coefficient of Variation
DEM	Discrete Element Method
DIC	Digital Image Correlation
DMA	Dynamic Mechanical Analysis
DOE	Design of Experiments
DSC	Differential Scanning Calorimetry
DSLR	Digital Single-Lens Reflex
DVE	Digital Video Extensometer
FDC	Fused Deposition of Ceramics
FEA	Finite Element Analysis
FFF	Fused Filament Fabrication
FRC	Fiber-Reinforced Composites
FRP	Fiber-Reinforced Polymer
IoT	Internet of Things
IR camera	Infrared Camera
ISO	International Organization for Standardization
LAAM	Large Area Additive Manufacturing
LED	Light Emitting Diode
LSAM	Large-Scale Additive Manufacturing
MEX	Material Extrusion
MF	Melt Flow
ML	Machine Learning
MPC	Material Property Characterization
PA	Polyamide
PC	Polycarbonate
PEKK	Polyetherketoneketone
PETG	Polyethylene Terephthalate Glycol
PLA	Polylactic Acid
PLC	Programmable Logic Controller
PP	Polypropylene
PPS	Polyphenylene Sulfide
ResNet	Residual Neural Network
ROI	Region of Interest
RVE	Representative Volume Element
RW	Review
SEM	Scanning Electron Microscopy
SFRC	Short Fiber-Reinforced Composite
SPH	Smoothed Particle Hydrodynamics
STL	Stereolithography
TMB	Thermal–Mechanical Behavior
μCT	Micro-Computed Tomography

Chapter 1
Introduction

Additive manufacturing (AM) has redefined contemporary fabrication methods by enabling the production of geometrically complex, functionally integrated, and highly customized components. Among the diverse AM modalities, Fused Filament Fabrication (FFF) is widespread, owing to its operational simplicity, material compatibility, and cost-efficiency [1], [2]. In this extrusion-based technique, a thermoplastic filament is incrementally melted and extruded through a nozzle to construct parts layer by layer, following a digital design. Its impact extends across sectors such as aerospace, biomedical applications, consumer products, and academic research [3], [4].

Despite its accessibility, FFF presents technical limitations, especially related to dimensional accuracy, mechanical consistency, and microstructural integrity. These challenges are associated with thermal gradients, anisotropic deposition patterns, and insufficient interlayer bonding, all of which influence final part performance [5], [6], [7]. A detailed understanding of these effects is important for improving the reliability and functionality of printed components.

Numerical simulations contribute to addressing these challenges by enabling virtual experimentation and process optimization. Thermal analyses capture the dynamic heat distribution during printing, providing insight into layer fusion and cooling behavior [8], [9], while mechanical models simulate stress evolution, deformation, and failure under loading [2], [10]. Recent developments have explored coupling these domains into thermo-mechanical models that consider time-dependent deposition, material behavior, and boundary interactions [11], [12]. However, many existing models still lack full experimental validation, and there is a recognized need for standardized testing and benchmarking to support predictive accuracy [13], [14].

Experimentally, the field has adopted optical tools such as Digital Video Extensometer (DVE) and Digital Image Correlation (DIC) to monitor strain and displacement. These non-contact techniques are helpful when characterizing brittle thermoplastics or anisotropic structures that may fail unpredictably [15], [16]. Nonetheless, repeatability across printed samples remains inconsistent, even when using ISO 527-1 standards, due to variables such as porosity, print orientation, and surface finish [7], [17]. This inconsistency complicates dataset comparisons and affects confidence in material qualification.

This thesis proposes an integrated approach combining numerical modeling and experimental evaluation to investigate the thermo-mechanical behavior of FFF-printed polymers. The objective is to develop and validate a modular framework for characterizing elastic and thermal responses, which may later support residual stress estimation and the study of fiber-reinforced composites. The first study presents a review of modeling strategies in the context of FFF, focusing on the numerical challenges of simulating fiber-reinforced polymers, where anisotropy, fiber orientation, and matrix-fiber interaction require more advanced approaches [4], [18], [19]. The review also identifies emerging research pathways such as simulation-in-the-loop control and AI-driven defect detection [20], [21], [22].

The second study applies a coupled numerical-experimental methodology to characterize PLA. The thermal simulation uses ANSYS's additive manufacturing environment to calculate temperature evolution based on a G-code-driven sequence of element activations, replicating the deposition process [14], [23]. The model incorporates process temperatures, baseplate preheating, and activation timing to emulate layer-by-layer heat transfer and cooling behavior. These data provide insights into thermal gradients and interlayer bonding conditions, which are known to influence the mechanical response of printed parts. A separate elastic finite element model replicates tensile test conditions, and strain data are obtained using DVE and DIC. This study also assesses test repeatability, boundary condition control, and optical tracking limitations [16], [24], [25].

While the initial focus is on PLA, the framework is intended to be extended to fiber-reinforced materials. These systems introduce added complexity due to the directional dependence of their thermal and mechanical properties, which makes integrated modeling especially relevant [4], [26], [27]. The proposed methodology also establishes a basis for incorporating residual stress prediction, fatigue analysis, and multiphysics simulations in future developments [6], [12], [23]. By emphasizing methodological consistency and cross-validation between simulation and experimental results, this thesis supports the development of transferable strategies for material characterization in extrusion-based additive manufacturing. The work is conducted within the scope of the NaturFAB project, which aims to promote sustainable, locally sourced AM practices by enabling robust material evaluation and process optimization across regional production networks.

1.1. Goals

This study aligns with several objectives of the NaturFAB project by establishing an integrated experimental–numerical methodology for the evaluation of components fabricated via Fused Filament Fabrication (FFF). The specific aims of this work are as follows:

- To review and critically assess current FFF simulation methodologies, identifying limitations in existing models related to melt flow, thermal behavior, stress development, and fiber–matrix interaction.
- To simulate the thermal behavior of PLA deposition using ANSYS Additive Manufacturing for a Directed Energy Deposition (DED) process, laying the groundwork for future incorporation of residual stress analysis into the numerical model and comparison with real-world results.
- To experimentally evaluate the tensile performance of PLA specimens fabricated via FFF, using DVE and DIC for non-contact strain measurement.
- To develop and validate a finite element model capable of accurately representing the elastic behavior of printed PLA under uniaxial loading, establishing a baseline for future simulation-experiment comparisons.
- To interpret incomplete or inconsistent experimental results as indicators of process variability, identifying key parameters that affect part integrity and measurement reliability.
- To provide a methodological basis for repeatable mechanical testing and reliable simulation, enabling future extension to fiber-reinforced composites and contributing to the development of standardized evaluation protocols for sustainable AM.

1.2. Work structure

This thesis is organized into four chapters:

Chapter 1 introduces the research context, motivation, and objectives, outlining the challenges in simulating and characterizing FFF-printed components and presenting the goals aligned with the NaturFAB project.

Chapter 2 presents a comprehensive literature review focused on numerical simulation strategies applied to Fused Filament Fabrication (FFF). It covers melt flow modeling, cooling and solidification behavior, thermo-mechanical analysis, and material property characterization, while also discussing simulation platforms such as Abaqus and Ansys. In addition, emerging trends, such as the use of fiber-reinforced composites and the integration of artificial intelligence for defect detection, are analyzed to identify current limitations and opportunities in the field.

Chapter 3 describes the simulation procedures and experimental methodology developed to evaluate the mechanical behavior of PLA specimens fabricated via FFF. It begins with a thermal analysis of the deposition process using the ANSYS Additive Manufacturing module, applying a DED strategy adapted to PLA printing. This simulation captures the thermal gradients during material deposition and serves as a basis for future residual stress assessments. Following the simulation, the chapter details the preparation of materials and specimens, tensile testing using DVE and DIC, and the construction and validation of a linear elastic finite element model. The results are analyzed to assess both the variability observed in printed specimens and the correlation between experimental and simulated data.

Finally, **Chapter 4** presents the global conclusions of the thesis and outlines future directions. It reflects on the practical implications of the findings in the context of the NaturFAB project, highlighting how the results support ongoing efforts to improve fabrication reliability, test repeatability, and numerical predictability in sustainable additive manufacturing workflows. Future work will focus on evaluating residual stresses generated during the printing process, both numerically and experimentally. These investigations aim to refine the simulation model and enhance its alignment with real-world behavior.

Chapter 2

A Comprehensive Review of Fused Filament Fabrication: Numerical Modeling Approaches and Emerging Trends [1]

Abstract: Fused Filament Fabrication (FFF) has become a widely adopted additive manufacturing technology due to its cost-effectiveness, material versatility, and accessibility. However, optimizing process parameters, predicting material behavior, and ensuring structural reliability remain major challenges. This review analyzes state-of-the-art computational methods used in FFF, which are categorized into four main areas: melt flow dynamics, cooling and solidification, thermal–mechanical behavior, and material property characterization. Notably, the integration of Computational Fluid Dynamics (CFD) and Finite Element Analysis (FEA) has led to improved predictions of key phenomena, such as filament deformation, residual stresses, and temperature gradients. The growing use of fiber-reinforced filaments has further enhanced mechanical performance; however, this also introduces added complexity due to filler orientation effects and interlayer adhesion issues. A critical limitation across existing studies is the lack of standardized experimental validation methods, which hinders model comparability and reproducibility. This review highlights the need for unified testing protocols, more accurate multiphysics simulations, and the integration of AI-based process monitoring to bridge the gap between numerical predictions and real-world performance. Addressing these gaps will be essential to advancing FFF as a precise and scalable manufacturing platform.

Keywords: Fused Filament Fabrication (FFF); Computational Fluid Dynamics (CFD); Finite Element Analysis (FEA).

---

[1] Enriconi, M. et al., 2025. A Comprehensive Review of Fused Filament Fabrication: Numerical Modeling Approaches and Emerging. https://doi.org/10.3390/app15126696.

2.1. Introduction

Additive manufacturing (AM), especially material extrusion (MEX), has changed how things are made by allowing the creation of complex geometries, reducing material waste by making parts that are almost the right size, and helping to create components designed for specific uses with special features. Among the various AM technologies, Fused Filament Fabrication (FFF) stands out due to its accessibility, ease of operation, and versatility in material selection [1]. This extrusion-based process involves the controlled deposition of a thermoplastic filament, which is heated to its melting point and deposited layer by layer to construct a three-dimensional object [3]. Its widespread adoption across industries such as aerospace, biomedical, and automotive engineering has led to an increasing demand for improved print quality, mechanical performance, and dimensional accuracy [2], [4].

Despite its advantages, FFF presents inherent challenges that impact part quality and reliability. Key factors such as thermal fluctuations, residual stresses, interlayer adhesion, and print parameters influence mechanical strength, dimensional stability, and surface finish [5]. These complicated details require numerical simulations, which provide predictive insights into material behavior, enabling the optimization of deposition strategies [8]. Computational models play a crucial role in analyzing melt flow dynamics, cooling and solidification, stress accumulation, and final material properties [28].

Two predominant simulation methods, Computational Fluid Dynamics (CFD) and Finite Element Analysis (FEA), are widely employed to model the FFF process [29]. CFD is often used to study how polymers flow and transfer heat, while FEA is used to determine the residual stresses, displacement and strain variation, and how well printed parts perform. The integration of these approaches has facilitated the development of more accurate predictive models, contributing to improved process control and part optimization.

Beyond traditional thermoplastics, recent advancements in fiber-reinforced composites have expanded the capabilities of FFF [30]. The incorporation of short and continuous fibers into polymer matrices has demonstrated significant improvements in mechanical strength, stiffness, and thermal stability, making FFF a viable solution for high-performance applications [4], [8], [18]. However, fiber integration introduces additional complexities, such as orientation control, dispersion uniformity, and interlayer bonding, requiring advanced numerical modeling techniques to optimize composite performance [28], [29].

In parallel, machine learning has emerged as a promising tool for improving FFF process reliability. Early efforts demonstrated real-time defect detection and interlayer quality prediction using AI-based models [20]. Recent studies have expanded these capabilities by integrating simulation-in-the-loop frameworks [21], thermographic imaging supported by machine learning [31], [32], and closed-loop control systems for adaptive process adjustment in fiber-reinforced printing [22]. These developments point to the growing role of intelligent, data-driven strategies in enhancing simulation fidelity, and defect mitigation in additive manufacturing.

In addition to summarizing current simulation strategies, this review aims to identify and articulate the main research gaps that limit the predictive capabilities of FFF modeling. These include the lack of standardized validation protocols, the limited integration of multi-scale and multi-physics models, and the scarcity of high-fidelity experimental data for benchmarking numerical predictions. Furthermore, the review highlights the emerging role of machine learning in process monitoring, inverse modeling, and real-time correction, which represents a promising direction for enhancing accuracy and automation in FFF simulations.

2.1.1. Meta-Analysis and Bibliometric Assessment

Bibliometric analysis and meta-analysis are essential tools for understanding the evolution of scientific research, identifying trends, and mapping interconnections between studies. In the context of numerical simulations applied to FFF, these methods provide a structured evaluation of academic progress, technological advancements, and the role of computational modeling in optimizing additive manufacturing processes [33]. As FFF processes become increasingly complex, numerical simulations play a key role in predicting material behavior, improving mechanical performance, and refining process parameters [2].

To evaluate this evolving landscape, a bibliometric analysis was conducted using a structured query applied to indexed databases. The search was designed to capture publications focused on fluid dynamics, structural modeling, and numerical methods within the scope of FFF. The query used was TITLE-ABS-KEY (additive AND manufacturing) AND TITLE-ABS-KEY (numerical AND methods) OR TITLE-ABS-KEY (numerical AND model) OR TITLE-ABS-KEY (simulation) AND TITLE-ABS-KEY (FFF) OR TITLE-ABS-KEY (FFF)

AND PUBYEAR > 2004 AND PUBYEAR < 2026. The resulting dataset included 743 publications, which were processed using Scopus, structured with Excel and Power BI, and analyzed through VOS viewer to identify thematic clusters and research trends.

A key focus of recent work has been the integration of fiber-reinforced polymers (FRPs) in FFF. From the initial dataset, ninety studies specifically addressed FRP-related simulations, examining the effects of short and continuous fibers on mechanical performance, deposition quality, and process optimization [5]. This thematic shift has gained momentum particularly since 2019 (**Figure 1**), reflecting both technological innovations and a growing interest in advanced composite materials. The bibliometric findings (see **Figure 2**) show a significant increase in research related to FRPs, indicating that this field is changing quickly and becoming more active within FFF simulation studies.

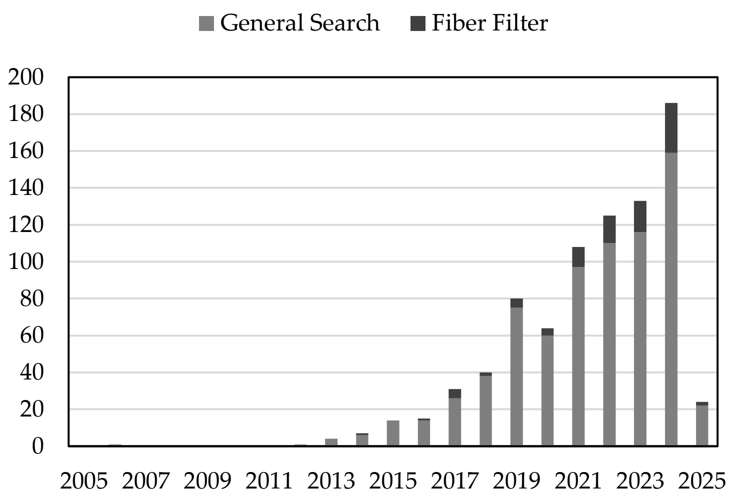

Figure 1. *Annual publications on FFF simulations (self-developed based on Scopus).*

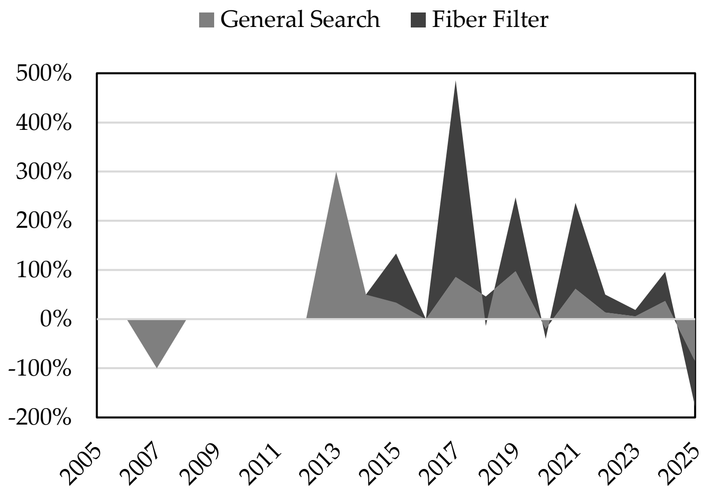

Figure 2. *Annual growth rate of FFF simulations (self-developed based on Scopus).*

The reviewed literature was split into four main research areas: melt flow dynamics, which studies how polymers act during extrusion and deposition; cooling and solidification, which looks at heat loss and how it affects layer bonding and leftover stress; thermal–mechanical behavior, which examines stress buildup, warping, and shape changes in printed objects; and material property characterization, which evaluates how different polymer mixes and fiber-reinforced materials affect the final strength of printed parts. To support this analysis, a co-word analysis using VOS viewer showed the importance and connections of the main research topics in the FFF simulation area. The resulting network (see **Figure 3**) highlights clusters of frequently co-occurring terms, such as material behavior, process parameters, and testing, reflecting the multidisciplinary nature of the field and the growing synergy between computational techniques and experimental investigation.

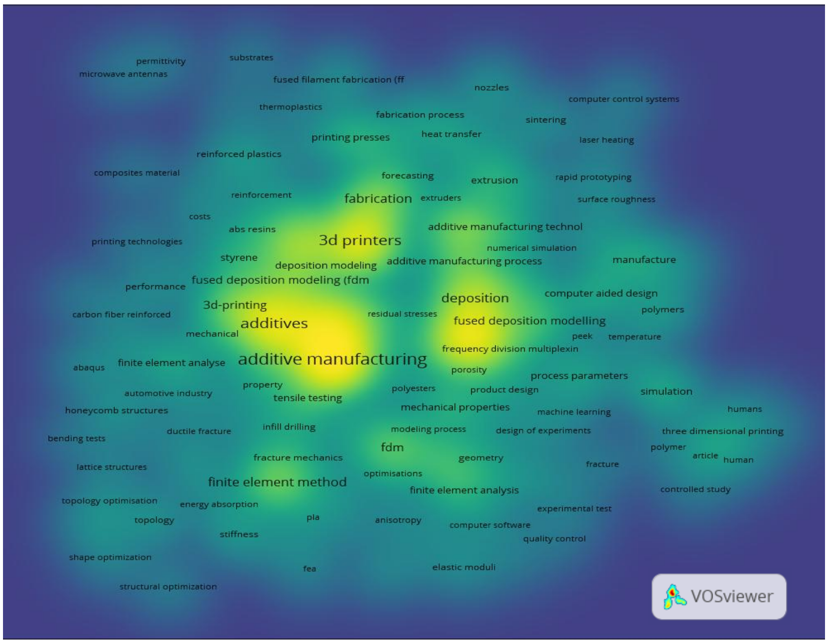

Figure 3. *Density of co-occurring keywords in FFF simulation research (self-developed based on Scopus).*

As the field grows, using detailed simulations, testing them in real life, and monitoring processes in real time will be crucial for making models more accurate and better at predicting outcomes. Future research should focus on creating consistent simulation methods, developing strong experimental testing techniques, and using machine learning to find defects, which will improve the accuracy, dependability, and scalability of FFF-based manufacturing processes. Future research should prioritize the standardization of simulation frameworks, the development of robust validation methodologies, and the incorporation of machine learning–based defect detection systems to enhance the precision, reliability, and scalability of FFF-based manufacturing processes.

2.2. Fused Filament Fabrication

2.2.1. Overview of the FFF Process

FFF is one of the most widely adopted extrusion-based additive manufacturing techniques, known for its affordability, accessibility, and material flexibility [34]. The process involves feeding a thermoplastic filament through an extruder, where it is heated, melted, and deposited layer by layer onto a build plate. A schematic of this setup is shown in **Figure 4**. This material deposition follows a digitally defined toolpath to construct three-dimensional parts with varying complexity. A computer-controlled motion system ensures the precise coordination of extrusion and movement, enabling consistent geometric accuracy.

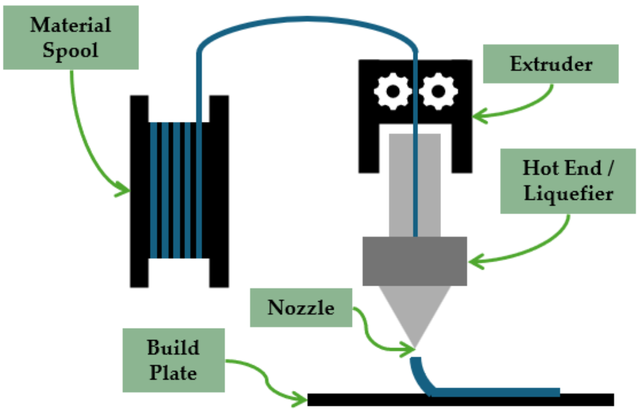

Figure 4. *Schematic representation of common setup in FFF (self-developed).*

The quality and mechanical performance of printed parts depend on process parameters, including extrusion temperature, layer height, print speed, raster orientation, and infill density. These variables directly influence outcomes such as interlayer bonding, dimensional accuracy, thermal gradients, and final part strength [35]. Commonly used FFF thermoplastics include Polylactic Acid (PLA), Acrylonitrile Butadiene Styrene (ABS), Polyethylene Terephthalate Glycol (PETG), and Nylon, each with distinct thermal and mechanical profiles [36]. In addition to these materials, recent studies have highlighted the growing relevance of semi-crystalline polymers such as polypropylene (PP), especially due to their attractive mechanical and chemical properties. However, their application in FFF presents distinct challenges, including high crystallization-induced shrinkage, reduced adhesion to the build surface, and a strong dependence of final properties on thermal gradients. To address these limitations, current research has proposed strategies such as optimizing the thermal environment, applying surface treatments, and incorporating crystallization kinetics into numerical simulation models [37], [38].

To accurately simulate or optimize this process, it is necessary to analyze the FFF workflow in discrete stages. Each phase involves distinct thermal, mechanical, and rheological phenomena that directly influence material behavior and part quality. In addition to polymer-based applications, FFF has also found widespread use in metal casting through the Lost-PLA technique. In this approach, printed PLA parts serve as sacrificial patterns in investment casting, enabling the production of intricate lattice and cellular structures that would be challenging to fabricate using conventional methods. Recent studies have demonstrated the effectiveness of this method for creating complex metallic components in aerospace and structural engineering contexts [39], [40]. Owing to its low cost and geometric flexibility, FFF is increasingly employed for prototyping and small-batch production in foundry environments.

2.2.2. Stages of Material Transformation in FFF

The FFF process encompasses a sequence of tightly coupled thermo-mechanical events, where the polymer undergoes physical, thermal, and rheological transformations that define the quality and performance of the printed part. The accurate modeling of these transformations has become essential to improve dimensional accuracy, optimize process parameters, and reduce manufacturing defects. A modular approach to simulation allows each stage of the process to be analyzed with dedicated tools and methodologies [2].

Figure 5 provides an overview of the main physical stages occurring during FFF. The filament is first melted and extruded through a heated nozzle, where it behaves as a viscous fluid and is deposited layer by layer according to a predefined path. This stage, governed by melt flow dynamics, is followed by cooling and solidification, in which the material transitions from molten to solid and interlayer bonding is established. As the structure grows, thermal gradients result in residual stresses, deformation, and potential warping, phenomena addressed through thermal-mechanical analysis. Finally, the mechanical and structural properties of the printed part are evaluated to determine whether it meets performance requirements, a step that often informs the design of new materials or reinforcement strategies. Each of these stages introduces distinct physical challenges that are targeted through specific numerical modeling strategies.

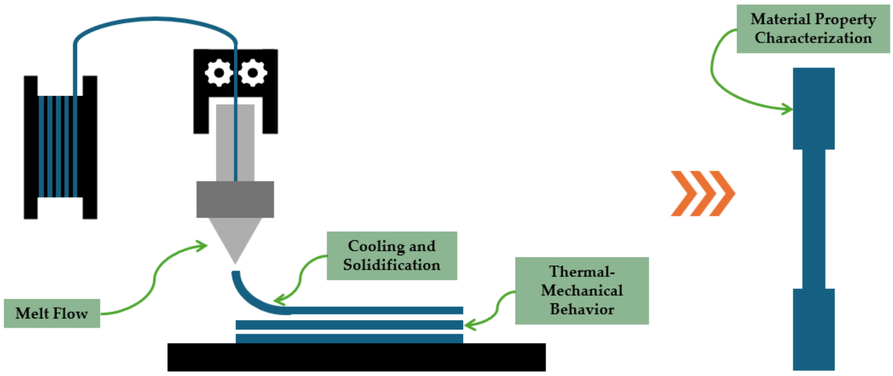

Figure 5. *Schematic representation of key physical phenomena in FFF (self-developed).*

In the following section, the focus is placed on the rheological properties of thermoplastics, which critically influence extrusion performance, flow stability, and material deposition during FFF.

2.2.3. Rheological Behavior of Thermoplastics in FFF

Rheology is the study of the deformation and flow properties of materials when subjected to external stress. In the FFF process, understanding the rheological behavior of molten thermoplastics within the heated die is essential for controlling process parameters and determining the quality of the printed part. In FFF, the filament feedstock is initially pulled by pinch rollers into the filament feed tube or directly into the heat break in the hot end. In this configuration, the filament acts as a continuous piston that pushes the molten material through the heated channel and the threaded nozzle onto the build plate [41]. The pressure required to extrude the melt is influenced by both the rheological behavior of the material and the geometric parameters of the print head. A failure in filament feeding can occur when the extrusion pressure exceeds the filament's ability to support the load, leading to buckling. In this context, the viscosity of the molten polymer determines the resistance to flow, while the compressive elastic modulus of the solid filament determines its ability to carry the compressive load [42].

The primary geometric parameters of the hot end include the inlet diameter (D1), corresponding to the filament size; the outlet diameter (D2) of the nozzle; the convergence angle (β); and the lengths of the extruder nozzle inlet (L1) and outlet (L2) channels [43]. These geometric factors influence the pressure decay along the flow path and therefore the extrusion force required. As illustrated in **Figure 6**, the molten polymer flows through four regions in the extrusion system. In the initial region (I), flow is pressure-driven within the hot end channel. At the center, both shear stress (τ) and shear rate ($\dot{\gamma}$) are minimal, while the axial velocity is maximal (*vz*). At the tube walls, the situation reverses, shear stress and shear rate reach their maximum values, while the velocity drops to zero [44]. This condition creates a shear gradient across the cross-section, where molecular orientation varies with the degree of shear. Molecules near the wall become increasingly aligned, while those at the center remain more disordered [45].

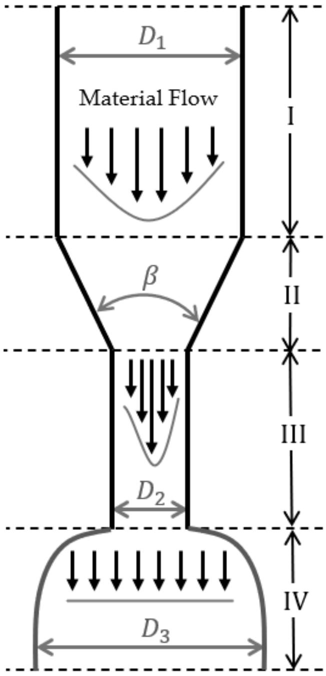

Figure 6. *Schematic illustration of the molten polymer flow profile and nozzle geometry, showing regions I–IV along the extrusion path. Based on Schramm [27].*

The mechanical behavior of this flow can be described by basic rheological equations that relate to stress and deformation under flow conditions. Shear stress (τ) is defined as the force applied (F) divided by the cross-sectional area (A) of the channel, expressed as: $\tau = F / A$. Shear rate ($\dot{\gamma}$), on the other hand, is defined as the velocity gradient across the radius of the flow channel, where *dvz* is the variation of axial velocity across the tube diameter and *dy* is the distance from the center of the tube, yielding: $\dot{\gamma} = dvz/dy$.

The polymer melt rheological behavior depends on the applied shear rate. At exceptionally low shear rates, typically below 10^1 s^{-1}, thermoplastics is considered a Newtonian fluid, exhibiting constant viscosity. In most polymer processing conditions, including FFF, shear rates fall between 10^1 and 10^5 s^{-1}, where the fluid exhibits non-Newtonian, shear-thinning (pseudoplastic) behaviors. At even higher shear rates, viscosity may plateau again, restoring Newtonian behavior [45]. **Figure 7** illustrates this relationship on a logarithmic scale. For FFF, shear rates within the nozzle are typically in the range of 100–200 s^{-1} [42]. Specifically for PLA, pseudoplastic behavior has been observed between 1 and 10^3 s^{-1} [46].

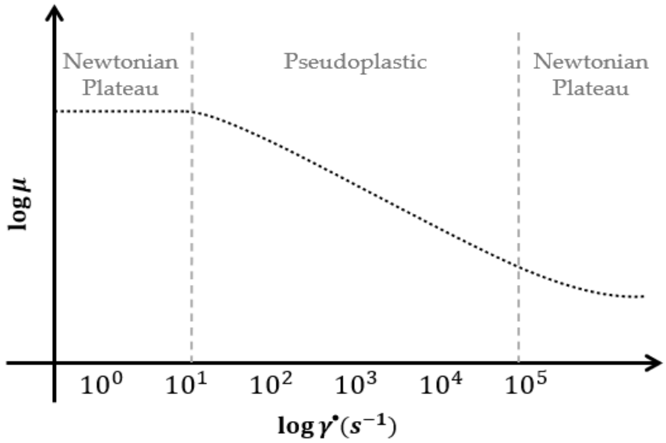

Figure 7. *Rheological behavior of molten thermoplastics, showing the variation of viscosity (μ) with shear rate (γ). Based on Manrich [28].*

This non-Newtonian behavior is described by the Power Law (Ostwald–de Waele) model, where k is the consistency index and n is the flow behavior index: $\tau = k.\gamma^n$. Mathematical models for simulating flow in FFF have used this equation [43]. A value of n = 1 indicates Newtonian behavior, while n < 1 characterizes pseudoplastic fluids [47]. The lower the value of n, the more pseudoplastic the material, resulting in a flatter flow front. The velocity profile shown in Figure 7 corresponds to a Newtonian fluid [48]. After region I, the molten polymer enters the convergent channel (region II), where the flow becomes elongational due to the change in cross-section. This behavior is analogous to the inlet region of a traditional extrusion die. In region III, the flow again becomes pressure-driven, but at increased velocity due to the smaller diameter. Upon exiting the nozzle (region IV), the flow profile does not present speed variation along the extrudate diameter, as the polymer enters at ambient pressure and undergoes relaxation, leading to an increase in diameter, a viscoelastic phenomenon known as extrudate swell (D3/D2 ratio) [44]. It is considered that the molten polymer undergoes an axisymmetric contraction flowing through the nozzle [49]. The cylindrical volume in the region of the inlet nozzle is elongated and its diameter is reduced; after it passes the convergent channel, it increases again at the nozzle outlet, reducing its length [44].

Molten polymers show a dependence on the speed, intensity, and time at which stress is applied, i.e., it is dependent on their thermo-mechanical history. They can partially return to their original shape after being stretched because their long molecular chains line up when stressed and then relax back to a random state when the stress is gone [48]. This behavior generates normal stress components when the polymer is out of the nozzle, which causes swell [45]. Whether in fluid or solid state, this behavior is called viscoelastic [50], as mathematical theories are applied in both cases [51]. The extent of extrudate swell depends on the thermo-mechanical history of the melt. The longer the residence time inside the nozzle, the greater the relaxation of elongational deformation and the smaller the residual contribution to swell. However, shear-induced elastic deformation within the nozzle still contributes to swelling. To mitigate this effect, it is recommended to reduce the extrusion speed, increase the processing temperature (at constant shear rate), increase the length-to-diameter ratio (L2/D2), and reduce the diameter ratio (D1/D2) [45], [51]. Other elastic effects during flow include melt fracture, shark skin, and draw resonance. These phenomena are caused by flow instabilities arising from elastic turbulence at the nozzle inlet, especially at high deformation rates in elongational flow, where stress levels exceed the cohesive strength of the polymer [48], [52].

Since viscosity is temperature-dependent, extrusion behavior is strongly influenced by thermal conditions. Excessively elevated temperatures can lead to discharge fluctuation and thermal degradation, while low temperatures increase viscosity and pressure demand, potentially resulting in melt fracture [48]. The average level of molecular orientation and residual stress in the printed part depends on three main factors: I) the shear-induced orientation during deposition; II) the relaxation time of the polymer chains (typically between 0.1 and 0.5 s for certain polymers); and III) the effective cooling time between processing temperature (Tp) and solidification temperature (Ts). This cooling time is determined by the size and geometry of the part, the polymer's specific heat, and the temperature intervals Tp–Ts and Tp–Tr, where Tr is room temperature [51]. The filament softens and melts in the heater block, which contains a machined flow channel. The melt quantity depends on the heat flux and material feed rate [41], [43]. The rate of thermal exchange is governed by the material's thermal diffusivity, which is determined by its conductivity, density, and specific heat [47]. As the temperature increases, viscosity decreases, reducing pressure drop and enhancing bonding between layers [43]. The pressure inside the die is controlled by variables: the geometry of the flow channel, the rheological properties of the melt, the temperature distribution, and the volumetric flow rate [52]. Material deposition is based on a constant volumetric displacement principle, where the flow rate is governed by the speed of the counter-rotating roller [41].

2.3. Numerical Simulation Applied to the FFF Process

Based on the stages illustrated in **Figure 5**, simulations are grouped into four categories: melt flow, cooling and solidification, thermal-mechanical behavior, and material property characterization [2]. Melt flow simulations focus on shear forces, viscosity variations, and flow stability, ensuring precise material deposition and interlayer bonding [13]. Cooling and solidification studies explore thermal gradients, heat dissipation mechanisms, and their effects on mechanical properties, which are key to preventing warping and structural defects [53]. Thermal–mechanical models predict stress distribution, distortion patterns, and deformation risks, aiding in process optimization and defect mitigation [1], [6]. Finally, material characterization simulations allow for the correlation between process parameters and final material properties, ensuring that predictions align with experimental validation [2].

The following sections provide an in-depth review of each numerical modeling domain, detailing key methodologies and significant findings that contribute to advancing FFF-based additive manufacturing.

2.3.1. Melt Flow

The melt flow behavior in FFF significantly influences the extrusion stability, the deposition accuracy, and the interlayer adhesion, which directly affect the mechanical properties and dimensional precision. Understanding polymer melt dynamics within the hot end, during extrusion, and after deposition enables control over print quality and the optimization of process parameters. CFD has advanced predictions of melt flow, specifically addressing viscosity effects, shear-induced deformation, and heat transfer processes.

Temperature and shear rate, closely related to extrusion speed, primarily govern the melt flow of thermoplastic materials during deposition. Due to the low pressures in FFF, these rheological factors dominate flow dynamics. Comminal et al. (2018) [54] developed a CFD model that considered polymer flow as an isothermal Newtonian fluid, demonstrating how filament geometry depends on nozzle-to-substrate gap and extruder-to-substrate velocity ratio. Their findings emphasize the precise control of deposition parameters to achieve optimal filament shape and interlayer adhesion. **Figure 8** shows how the strand shape (W/H) and density (A/(W·H)) change based on the distance from the nozzle to the surface (g/D) and the speed of the material flow (V/U). As g/D increases, the aspect ratio decreases, indicating a wider and flatter strand profile, while the compactness is maximized at intermediate V/U values, reflecting the interplay between shear rate and material deposition behavior.

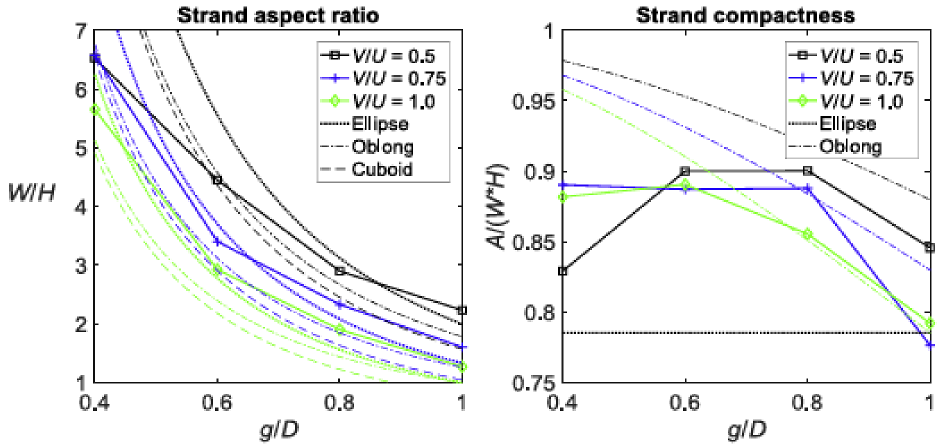

Figure 8. *Aspect ratio (W/H) and compactness (A/(W·H)) of the deposited strand as functions of the normalized nozzle gap (g/D) and velocity ratio (V/U). Adapted with permission from [54].*

Building on their earlier findings, Serdeczny et al. (2022) [55] developed an advanced CFD model, incorporating viscoelastic rheology to simulate the non-isothermal polymer flow more accurately through the hot end in filament-based additive manufacturing. Unlike previous models that assumed fully liquefied flow or employed generalized Newtonian approximations, this approach accounted for shear and elongational stresses, offering improved predictive accuracy for filament feeding forces across varying process conditions. The model was experimentally validated and demonstrated strong alignment with measured data, particularly under high flow rates. Furthermore, it enabled the parametric optimization of key hot-end geometries, such as liquefier length, capillary diameter, and inlet angle, highlighting their impact on flow stability and extrusion performance. These findings reinforce the earlier conclusions by Serdeczny et al. (2020) [56], who identified recirculation regions at the solid–melt interface as critical factors that influence temperature distribution and pressure buildup within the nozzle, underscoring the importance of physically representative rheological modeling (**Figure 9**).

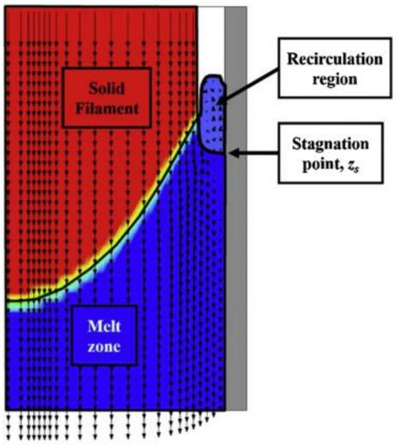

Figure 9. *Sketch illustrating the definition of the solid filament, recirculation region, stagnation point, and melt zone. Adapted with permission from [55].*

Nozzle design plays a fundamental role in controlling melt flow dynamics in extrusion-based additive manufacturing. Jeong et al. (2021) developed a nozzle modification strategy aimed at controlling the orientation of filler particles during extrusion [57]. By embedding an orifice geometry into the nozzle, they induced the perpendicular alignment of anisotropic reinforcements, which directly influenced the mechanical anisotropy of printed parts. Through combined experimental and numerical analysis, the study demonstrated how nozzle-induced flow fields affect particle orientation, highlighting the importance of microstructural control in melt flow modeling and the functional optimization of fiber-reinforced filaments [56].

Building on this notion of nozzle-function tailoring, Schuller et al. (2024) [58] employed CFD simulations coupled with global optimization algorithms to improve nozzle geometry for high-speed FFF applications. By parameterizing the nozzle profile using spline curves and enforcing manufacturability constraints, they identified geometries that significantly reduce pressure drops while maintaining effective flow characteristics. Experimental validation confirmed these findings, demonstrating that optimized nozzles, particularly the organic and PET-G-specific designs, lowered pressure drop by up to 67%, with reduced backflow and improved extrusion force control. These results emphasize that tailoring nozzle design to polymer rheology can directly enhance printing performance, precision, and throughput, employing nozzle optimization as a valuable tool in the advancement of FFF processes (see **Figure 10**).

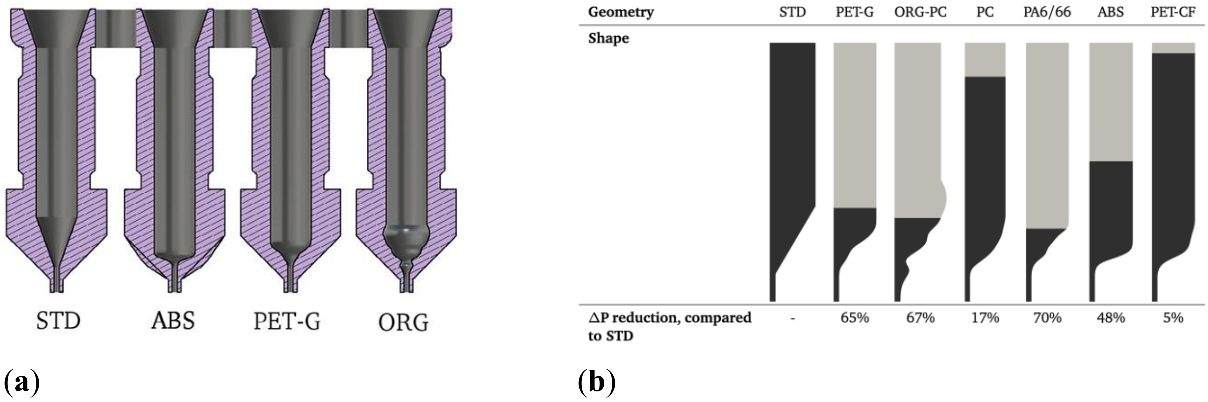

Figure 10. *Nozzle geometries (a) and pressure drop reduction per geometry compared to the standard nozzle (b), with values obtained from simulations and experimental validation. Adapted with permission from [58].*

At high extrusion speeds, melt flow presents additional complexities. Phan et al. (2020) [46], through CFD simulations in ANSYS Fluent, observed that rapid extrusion reduced the heating period, resulting in incomplete polymer melting, filament distortion, and decreased accuracy. They indicated that current numerical models fall short under high-speed conditions and recommended developing advanced thermal and rheological models to improve predictive accuracy. This limitation is closely tied to the viscoelastic nature of polymer flow at elevated deformation rates, particularly during elongational deformation in the nozzle. **Figure 11** presents the pressure drop of PLA melt as a function of shear rate, measured using both capillary and orifice dies. The steep increase in pressure drop with shear rate underscores the dominance of elongational effects in high-speed extrusion and supports the adoption of the Phan–Thien–Tanner (PTT) model to predict flow resistance more accurately under these conditions. These experimental insights validate the simulation observations and highlight the need for rheological models that capture pseudoplastic behavior when aiming to scale FFF processes to higher speeds.

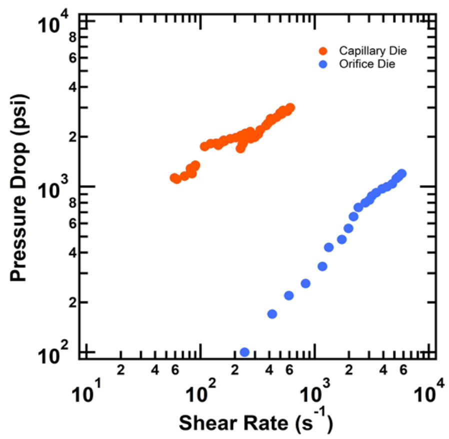

Figure 11. *Pressure drops of PLA as a function of shear rate, measured using capillary and orifice dies. Adapted with permission from [46].*

Collectively, these studies indicate that melt flow behavior in FFF strongly depends on extrusion conditions, including nozzle temperature, feed rate, and layer height. CFD-based approaches effectively characterize flow instabilities, optimize deposition, and enhance interlayer bonding. Nevertheless, melt flow alone does not solely determine the mechanical properties of printed components. Post-deposition cooling and solidification introduce thermal dissipation and phase transitions that significantly impact residual stresses and structural stability. The subsequent section explores these thermal mechanisms and their role in interlayer adhesion, mechanical strength, and dimensional accuracy in FFF.

2.3.2. Cooling and Solidification

The cooling and solidification phase in FFF is designed to achieve optimized interlayer adhesion, mechanical performance, and dimensional accuracy (Liparoti et al., 2021) [59]. Removing heat properly during the polymer deposition process helps to create strong bonds between layers by allowing effective molecular diffusion. Therefore, it is necessary to control the heat transfer mechanisms (conduction, convection, and radiation) to maintain structural integrity and ensure high-quality printed components. Among these mechanisms, conduction has been identified as the dominant heat transfer mode. Costa et al. (2014) [9] confirmed that conduction between deposited filaments and the build plate significantly outweighs convection and radiation in cooling efficiency. They recommended strategies such as preheating the build surface or controlling chamber temperatures to effectively reduce thermal gradients, thereby minimizing warping and delamination.

Heat transfer also determines the quality of filament bonding. Zhang et al. (2017) [60] developed a 3D transient thermal model and found that reheating from newly deposited layers improved molecular entanglement, whereas rapid cooling negatively impacted interlayer strength. In addition to the thermal findings, their study employed the *Element Birth and Death* technique in ANSYS to simulate the sequential nature of layer deposition. This approach allowed the model to dynamically activate elements as new material was added, accurately capturing the temporal evolution of the thermal field and heat accumulation across layers. As a result, the simulation provided enhanced insight into local reheating effects, cooling gradients, and the influence of deposition timing on interlayer temperature history. Similarly, Zhou et al.

(2016) [61] used FEA, which considers how materials behave at different temperatures, and found that quick cooling is harmful because it limits how materials can mix, weakens their stickiness, and raises internal pressures. To optimize bonding quality, they recommended controlling cooling rates through adjustments in build plate temperature and using enclosed printing environments.

Further deepening the understanding of adhesion, Coogan and Kazmer (2017) [62] developed a diffusion-based healing model, emphasizing maintaining interfacial temperatures above the polymer's glass transition temperature (Tg) to enhance polymer chain diffusion effectively. Similarly, Lepoivre et al. (2020) [63] utilized infrared thermography and thermal simulations to explore heat transfer and adhesion during FFF. They demonstrated that filament adhesion depends heavily on coalescence and polymer chain reptation, the thermal motion of polymer chains that allows them to entangle and effectively bond. Both phenomena are driven by the thermal history experienced during the process. Their findings indicate that precise thermal management, particularly accurate control over the cooling rate, significantly enhances mechanical performance, especially in high-performance thermoplastics such as PEKK (see **Figure 12**).

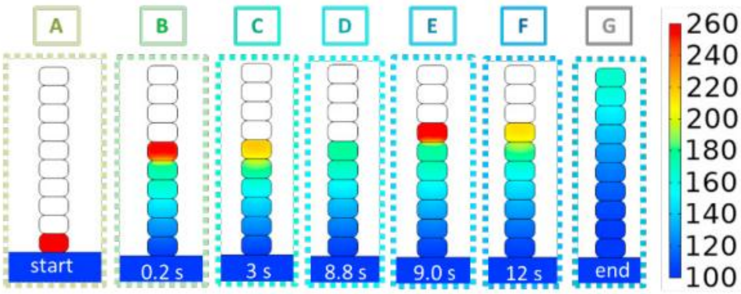

Figure 12. *COMSOL model showing the temperature evolution (°C) for ABS during the extrusion process. Adapted from [63].*

Addressing practical constraints, Go et al. (2017) [20], [64] identified key limitations such as extrusion force, heat transfer efficiency, and printhead motion in FFF. Their results indicated that elevated nozzle temperatures enhance extrusion speeds but are limited by insufficient thermal conduction within the filament core, increasing extrusion forces and the risk of filament buckling. To address this, they suggested longer liquefiers to enhance heating efficiency, enabling higher flow rates without excessive force. These thermal limitations are further illustrated in **Figure 13**, where finite element simulations show that, as flow rate increases, heat penetration into the filament core decreases significantly, especially near the liquefier inlet. At higher build rates, core temperatures drop, highlighting the reduced thermal residence time.

These findings support the recommendation to implement extended heating zones and underscore the critical role of balanced thermal management in ensuring efficient material flow and preventing mechanical instabilities during the printing process.

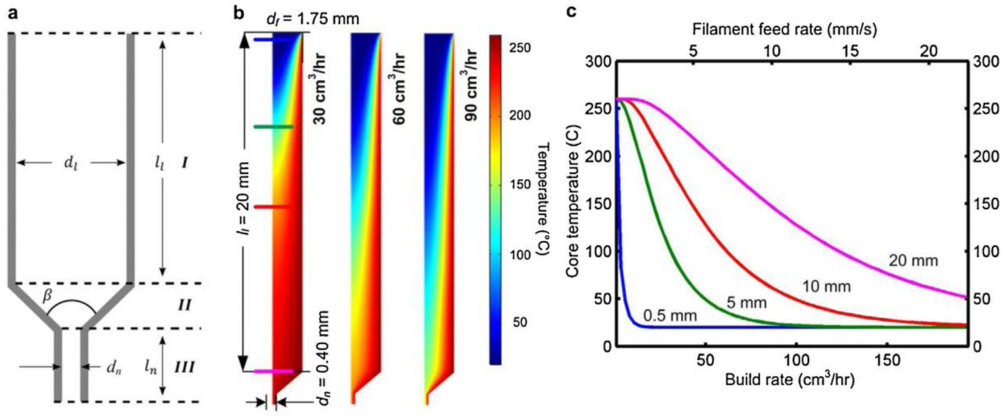

Figure 13. *Heat transfer within the liquefier: (a) geometric regions: heater tube, constriction, and nozzle; (b) temperature distribution at volumetric flow rates (c) core temperature as a function of build rate. Adapted with permission from [64].*

Enhancing print reliability, Jin et al. (2020) [20] developed an AI-based real-time monitoring system using computer vision and embedded strain sensors to promptly detect interlayer defects such as warping and delamination. Their system successfully identified defects early, significantly improving reliability and reducing material waste. The relationship between cooling dynamics and residual stress generation further clarifies the role of thermal management in FFF. Xia et al. (2018) [65] employed CFD simulations to reveal that uneven cooling leads to differential thermal contraction, causing localized stresses and dimensional inaccuracies. By incorporating temperature-dependent shrinkage models, their simulations improved predictions of residual stresses. Extending these findings, Serdeczny (2020) [66] developed a comprehensive numerical model, indicating that the rapid cooling near the nozzle exit increases residual stresses, resulting in geometric distortions. Experimental validation confirmed that higher extrusion temperatures enhance adhesion but simultaneously increase the residual stress of thermal origin.

Together, these studies underscore the role of temperature evolution in determining bonding quality and dimensional outcomes during FFF. However, the development of internal stresses resulting from non-uniform cooling and constrained thermal contraction cannot be fully explained by thermal considerations alone. To address this, the following section focuses on how residual stress accumulation and thermally induced deformation evolve during the printing process, and how they influence the structural integrity and reliability of FFF-manufactured parts.

2.3.3. Thermal-Mechanical

Thermal-mechanical behavior in FFF involves the interaction between thermal gradients, material shrinkage, and mechanical constraints imposed by the layered manufacturing process. These interactions lead to the development of residual stresses and strain localization, which can result in defects such as warping, delamination, or dimensional instability. Numerical approaches typically address these effects by coupling transient thermal simulations with mechanical models that incorporate temperature-dependent material properties and layer-by-layer deposition sequences.

One of the earliest mathematical models for warp deformation in FFF was developed by Wang et al. (2007) [67], who analyzed thermal stresses induced by material contraction during cooling. Their study examined the influence of deposition layer count, section length, chamber temperature, and material shrinkage rate on deformation. They found that higher chamber temperatures reduce warp deformation, while larger stacking sections and higher shrinkage rates increase it. Their model provided valuable insights into process optimization, emphasizing that adjusting raster angles and partitioning deposition areas can significantly improve dimensional accuracy. However, the model does not fully account for residual stress evolution during cooling or the effects of complex geometries, limiting its applicability for intricate parts.

To expand simulation capabilities and reduce computational demands, Bhandari and Lopez-Anido (2020) [68] introduced a discrete-event thermal model capable of capturing transient heat transfer behavior during the printing process. Their approach demonstrated good agreement with more computationally intensive methods, making it suitable for efficient thermal prediction across various geometries and parameter settings. More recently, Jiang (2023) [69] developed a high-fidelity thermal simulation framework specifically aimed at improving the prediction of temperature fields and guiding the process optimization of printed polymer and composite parts. The study emphasized the importance of accurately capturing spatiotemporal temperature gradients to mitigate stress concentrations and improve structural performance.

Building on earlier findings, advanced finite element approaches have been developed to simulate stress accumulation and deformation in FFF. Morvayová et al. (2023) [23] developed a 3D thermo-mechanical finite element model to predict dimensional accuracy, defect formation, and residual stresses in wood/PLA biocomposites fabricated via FFF. Their study identified uneven filler distribution and high hydrophilicity as major challenges, influencing printability and final part stability. The model, validated experimentally, demonstrated that residual stresses are sensitive to layer thickness and extrusion temperature. As shown in **Figure 14**, residual stress increased significantly with thicker layers, with values peaking at 48 MPa for 0.25 mm layer thickness. Lower nozzle temperatures and thinner layers resulted in reduced thermal gradients and lower residual stress values, especially in the lower portions of the parts, which remained more constrained by platform adhesion. These findings reinforce the need to optimize process parameters, especially for heterogeneous biocomposites, and highlight current limitations in capturing anisotropic thermal–mechanical interactions in such materials.

Another finite element modeling approach was developed by Cattenone et al. (2018) [14], who used ABAQUS to predict distortions in FFF with a sequential element activation method. Their study showed that smaller time steps improve temperature accuracy but have minimal effect on residual stress, while finer meshing improves stress gradient predictions but significantly increases computational cost. Their model was validated against experimental data for a planar spring and a bridge model, showing good agreement, with vertical displacement errors of 23% and 12%, respectively. However, the study highlighted the need for better adhesion models to capture first-layer interactions and improved methods for predicting part detachment and warping behavior.

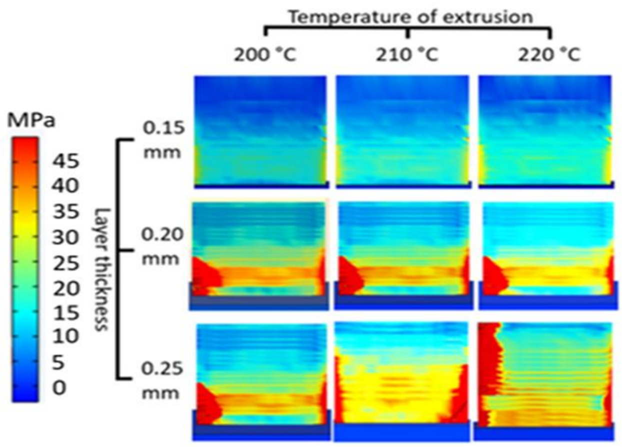

Figure 14. *Residual stress distribution in FFF-manufactured PLA/wood biocomposite cubes with varying layer thicknesses and extrusion temperatures. Adapted with permission from [14].*

The impact of temperature variations on residual stress and part deformation was also investigated by El Moumen et al. (2019) [11], who developed a 3D thermo-mechanical model to predict temperature gradients, residual stresses, and delamination in FFF-printed polymer composites. Their results showed that rapid temperature changes between layers increase stress concentrations, raising the risk of delamination. Their analysis also found that filament deposition produces higher temperature gradients than layer-by-layer printing, leading to more distortion and stress accumulation. Experimental validation showed temperature deviations below 5%, confirming the model's accuracy. However, they emphasized the need for better modeling of anisotropic mechanical behavior and complex thermal interactions to improve stress predictions.

These studies jointly confirm that residual stresses and thermal deformations remain significant challenges in FFF, requiring a combination of multi-scale modeling and optimized print parameters to mitigate these limitations. The next section will explore the role of material properties and their characterization, detailing how processing conditions, fiber integration, and post-processing techniques influence final part performance.

2.3.4. Material Property Characterization

The mechanical and thermal behavior of materials in FFF depends on process parameters, material composition, and reinforcement strategies [13]. Factors such as layer thickness, infill density, raster orientation, and cooling rate influence strength, ductility, and failure mechanisms in printed parts [18]. To optimize material performance and structural integrity, researchers have combined experimental testing, numerical modeling, and real-time defect detection to evaluate how printing parameters affect mechanical behavior.

The influence of printing parameters on mechanical properties has been studied. Croccolo et al. (2013) [70] and Domingo-Espin et al. (2015) [15] investigated the mechanical behavior of parts produced via FFF, focusing on ABS-M30 and Polycarbonate (PC), respectively. Both studies concluded that strength and stiffness were highest when filament layers were aligned with the loading direction, whereas perpendicular loading resulted in weaker performance due to reduced interlayer bonding. Analytical and finite element models developed by these authors closely matched experimental results, achieving average deviations below 10%. However, both studies emphasized the need for improved modeling to better capture plastic deformation and failure behavior beyond the elastic limit. The experimental and numerical configurations used by Domingo-Espin et al. are illustrated in **Figure 15**.

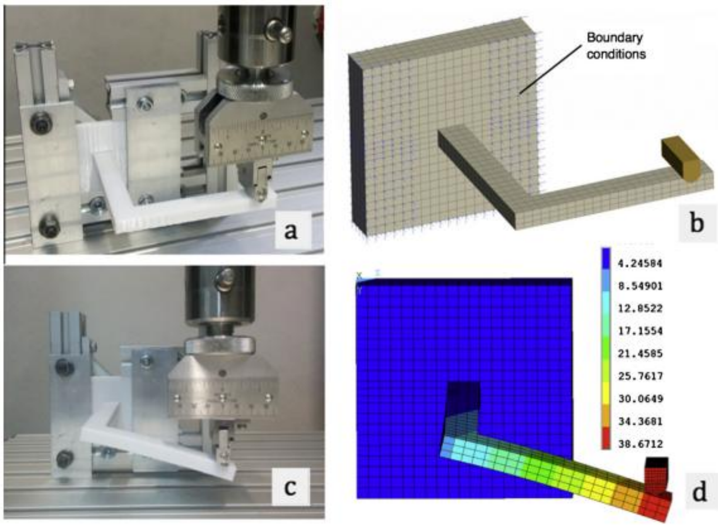

Figure 15. *Experimental setup for the physical test (left) and ANSYS® simulation schematic (right). Small displacement views (a,b), and images at 35 mm of deformation (c,d). All dimensions in millimeters. Adapted from [15].*

In addition to mechanical performance, geometric accuracy and surface quality are crucial for material characterization. García Plaza et al. (2019) [7] studied how build orientation, layer thickness, and feed rate affect PLA part dimensions, flatness, and surface texture. Thinner layers improved dimensional accuracy, while feed rate had minimal impact. Flatness errors primarily resulted from variations in layer thickness and extruder acceleration/deceleration, with higher feed rates increasing material accumulation. Surface roughness increased with thicker layers due to the stair-stepping effect inherent in layered manufacturing. The study highlighted the importance of precise extruder control and optimized parameters for better surface quality and geometric accuracy.

A simplified numerical model was proposed by Zouaoui et al. (2021) [16] to predict the mechanical behavior of FFF 3D printing parts that are built from an ABS pre-structured material. The model effectively addresses the anisotropic build configuration by assigning local material reference frames to individual mesh elements. It treats the material as homogeneous and employs specific material constants to introduce anisotropy associated with intricate deposition trajectories. Their results verify that the material exhibits quasi-isotropic elastic behavior, as the longitudinal and transversal Young's modulus are approximately equivalent. The strength anisotropy in tensile specimens with varying raster angles has been determined by combining Hill's criterion with the filament's plastic flow curve. The longitudinal direction possesses the highest yield strength and a ductile behavior, whereas the transversal direction is the weakest and demonstrates fragile behavior at the yielding point. These effects are quantitatively illustrated in the comparison between simulated and experimental load–displacement curves shown in **Figure 16**.

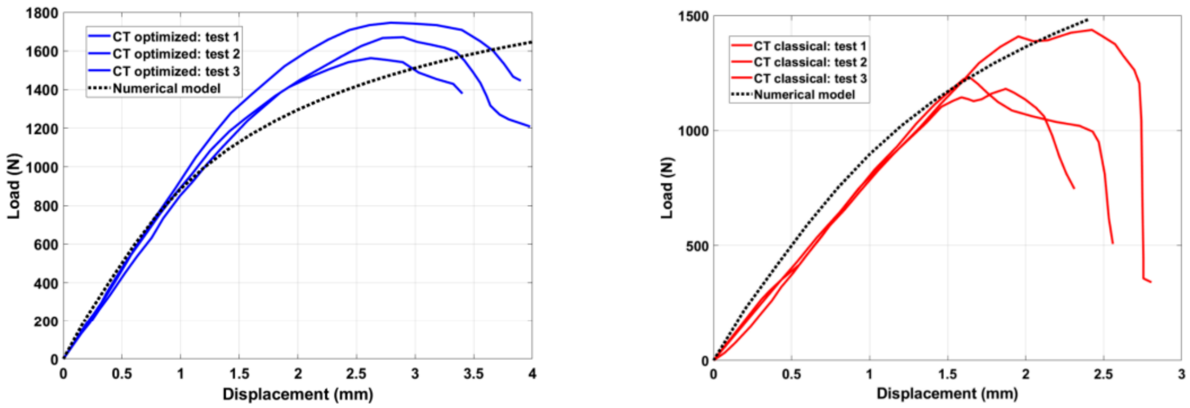

(a) (b)

Figure 16. *Load–displacement curves from CT tests. (a) Classical samples printed with ±45° raster orientation; (b) Optimized samples with filament aligned along the principal stress direction. Adapted from [16].*

Advancing such models requires precise experimental characterization to obtain reliable and process-relevant material data. Dynamic Mechanical Analysis (DMA) provides viscoelastic properties, such as storage and loss moduli across a range of temperatures, that are commonly used to model stress relaxation and residual stress evolution [71]. Differential Scanning Calorimetry (DSC) is widely applied to identify thermal transitions, including glass transition temperature (Tg), melting point (Tm), and crystallinity, which affect shrinkage and stiffness, particularly in semicrystalline polymers like PLA and PA. Additionally, micro-computed tomography (micro-CT) allows the non-destructive, high-resolution imaging of internal porosity, fiber distribution, and interlayer adhesion. These structural insights support the validation of mesoscale simulations and help to relate internal features to mechanical behavior [72].

Material failure mechanisms have also been studied extensively. Garg and Bhattacharya (2017) [25] conducted FEA and experimental tests to study the effect of raster angle and layer thickness on tensile failure. They found that thinner layers improve elongation and load-bearing capacity due to the higher number of load-aligned layers, while thicker layers result in higher tensile strength because of fewer air voids and stronger interlayer bonds. **Figure 17** illustrates the stress distribution across samples with different raster angles and layer thicknesses. Specimens with 0° rasters exhibit more uniform stress distribution along the loading direction, while those with 90° rasters show stress localized at the interlayer regions, leading to early delamination. In 0°/90° raster configurations, failure typically initiates in the 90° layers and propagates through the structure, ending in brittle fracture of the 0° layers. These results highlight the need for refined models that can better capture interlayer bonding behavior and failure progression in anisotropic printed parts.

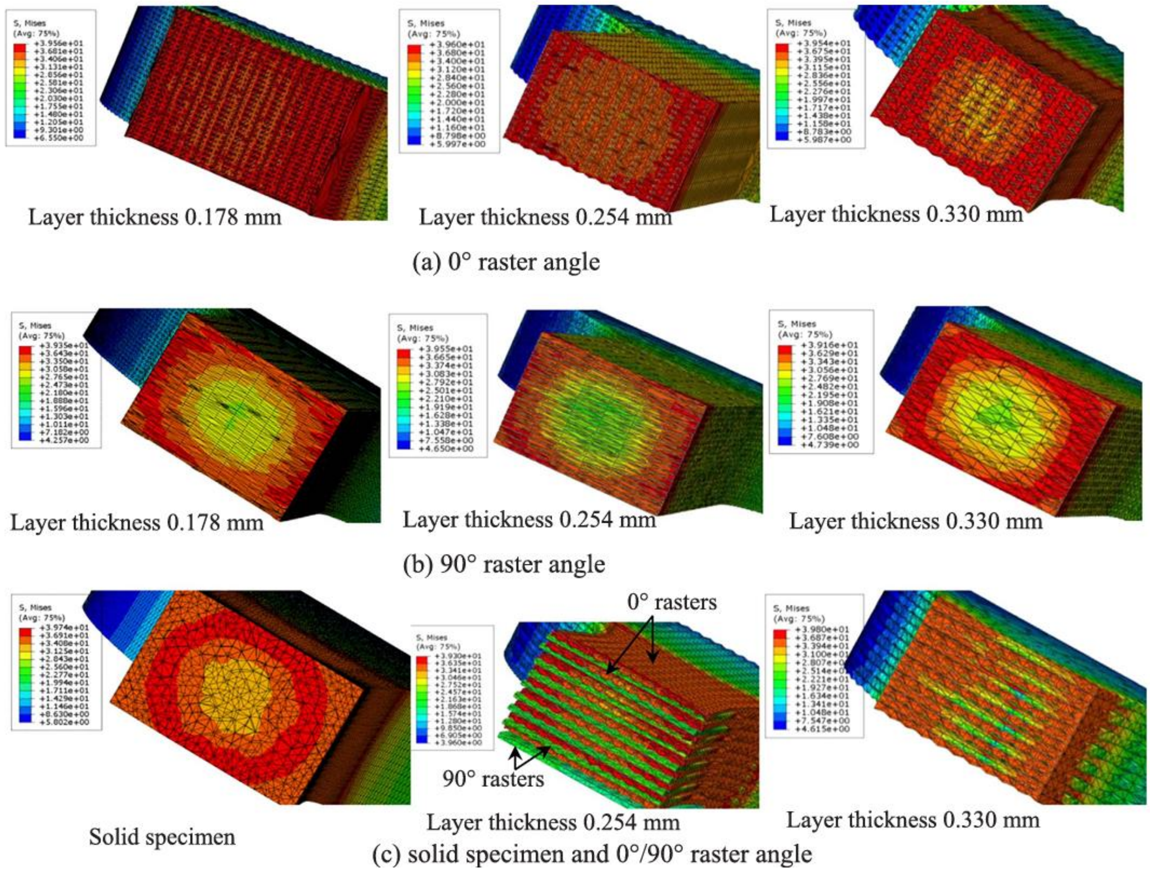

Figure 17. *Cross-sectional stress distributions from FE simulations of FFF specimens with different layer thicknesses and raster angles, including a solid specimen. Adapted with permission from [25].*

Expanding on anisotropy in AM, Dai et al. (2025) [10] reviewed the mechanical behavior of additively manufactured materials, focusing on how the layer-by-layer process creates structural heterogeneity, residual stress, and defects. Their analysis found that materials, process parameters, and post-processing techniques all influence anisotropic behavior, with metals, polymers, and composites responding differently. Crystal plasticity models accurately predict anisotropy in metals, but polymer models often oversimplify microstructural effects. They emphasized the need for improved modeling approaches that integrate machine learning and multiscale physics but noted that many current models lack validation across different AM processes, highlighting the need for better experimental benchmarking and real-time simulation improvements.

To improve failure detection, Fu et al. (2025) [21] developed a simulation-in-the-loop framework for real-time structural validation in AM. Their system combines FEA with in situ defect detection, using a U-net image segmentation model to analyze defects layer by layer. Experimental tests on a material extrusion printer demonstrated that the framework could predict failure strength within 5% accuracy, allowing for early defect detection and automated print termination when necessary. They found that defect size and distribution directly influence stress accumulation, but computational efficiency remains a challenge in complex geometries and high-speed printing. The progression of strain distribution in a defective sample under tensile loading is illustrated in **Figure 18**.

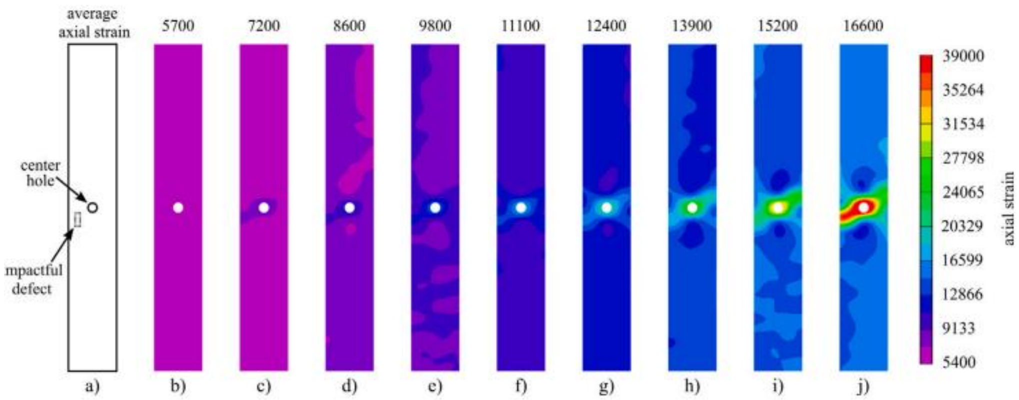

Figure 18. *Strain distribution progression in a sample with an internal defect subjected to tensile loading. The sequence shows the evolution from the initial unloaded state to post-fracture, highlighting the average axial strain. Adapted from [21].*

To further enhance failure prediction and quality assurance in FFF, thermography-based approaches have also been explored. Rodríguez-Martín et al. (2020) [31] demonstrated the use of active thermography supported by machine learning to predict internal defects in polymer-based additively manufactured components. Their methodology enabled the non-destructive, real-time identification of internal flaws from thermal sequences, improving process monitoring and reliability. Building on this, Rodríguez-Martín et al. (2022) [32] employed step-heating thermography in combination with simulation and ML models to accurately estimate internal defect sizes. Their results underscore the potential of integrating thermal diagnostics with data-driven techniques to support in situ structural validation and quantitative defect characterization. These contributions reinforce the growing relevance of hybrid experimental–computational methods in advancing defect-aware modeling for FFF.

However, despite their potential, current validation strategies still face critical gaps. Traditional methods, such as mechanical testing under simplified geometries [15], [70] or dimensional accuracy analysis [7], often neglect microstructural irregularities and transient thermal effects. Techniques like micro-computed tomography (μCT) [72], simulation-in-the-loop validation [21], and thermography supported by machine learning [31], [32] have improved the ability to detect and quantify internal defects, but their adoption remains limited due to equipment costs, a lack of standardized protocols, and challenges in integrating experimental data into numerical frameworks. Therefore, advancing reliable FFF simulation will require the broader implementation of high-fidelity, non-destructive validation tools and coordinated efforts to establish shared benchmarks across materials, geometries, and simulation platforms.

Building on this foundation, future research should prioritize advanced modeling techniques capable of capturing anisotropy, residual stresses, and defect formation more effectively. Integrating machine learning with multi-scale physics-based simulations and real-time process monitoring could significantly enhance predictive accuracy and efficiency. In the next section, the influence of fiber reinforcement on material performance is examined, specifically addressing how fiber type, orientation, and distribution impact composite properties.

2.4. Fiber-Reinforced Composites

Most polymers employed in Fused Filament Fabrication (FFF) exhibit inherently low mechanical properties; one effective strategy to enhance their performance is reinforcement with fibers. Integrating fiber reinforcements into thermoplastic matrices significantly improves mechanical strength, dimensional stability, and thermal performance in FFF [73], [74]. Short fiber-reinforced composites (SFRCs), commonly carbon, glass, or natural fibers, improve stiffness and moderately increase strength, but their properties remain anisotropic due to random fiber orientations. Continuous fiber-reinforced composites (CFRCs) provide superior mechanical properties comparable to polymeric materials but require precise fiber alignment and controlled deposition, complicating the printing process.

Yang et al. (2017) [75] developed a coupled Smoothed Particle Hydrodynamics (SPH) and Discrete Element Method (DEM) model to simulate the 3D printing process of fiber-reinforced polymers. Their study explored the behavior of both short glass fibers in ABS and continuous carbon fibers in Nylon during extrusion. As shown in **Figure 19**, short fibers tend to align with resin flow, but interactions near the nozzle walls can introduce chaotic movement and reduce alignment. In contrast, continuous fibers remain centered early in the extrusion but undergo significant bending deformation and stress buildup as printing progresses. This deformation, along with fiber-nozzle contact, can lead to tool wear and performance reduction. The model also demonstrated how nozzle geometry and extrusion velocity influence flow fields and fiber positioning. Although the model lacked thermal and shrinkage considerations, it provided valuable insights into fiber-resin interactions and established a foundation for multi-physics simulations.

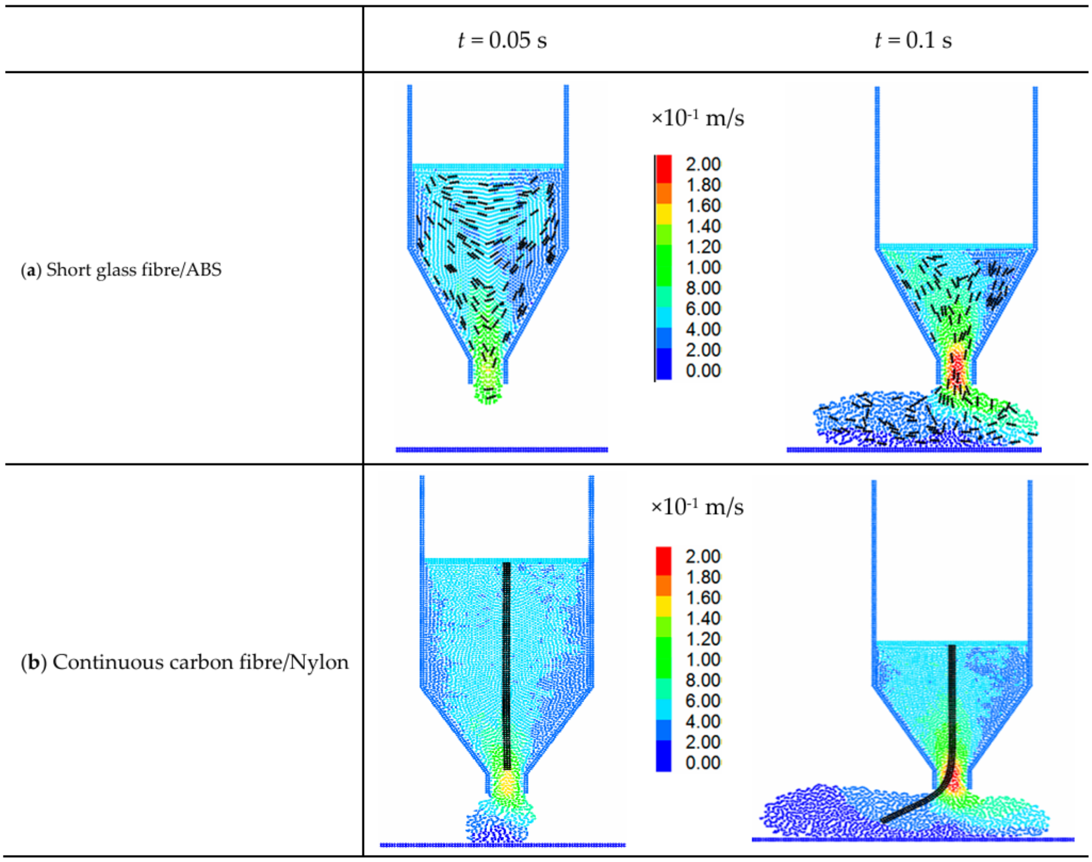

Figure 19. *(a) Short glass fiber/ABS composites show chaotic flow-induced reorientation; (b) Continuous carbon fiber/Nylon composites exhibit bending and stress concentration due to interaction with nozzle walls. Adapted with permission from [75].*

Yang et al. (2022) [26] further studied fiber breakage and orientation experimentally using X-ray micro-computed tomography (μCT), finding that smaller nozzles increased fiber breakage and larger layer heights improved alignment but increased porosity, thus decreasing tensile strength. Their results highlighted critical trade-offs between fiber integrity and mechanical performance.

Topology optimization has emerged as an effective approach for improving composite performance. Yang et al. (2022) [76] developed a topology optimization method aligning fiber paths with stress distributions, improving stiffness-to-weight ratios and manufacturability. Experimental validations confirmed improvements but emphasized the need for better fiber continuity and optimized path planning. Yap et al. (2024) [27] similarly demonstrated that topology optimization improved stress distribution and structural performance compared to shape optimization, although defects and fiber misalignments from manufacturing processes indicated that models should better reflect practical constraints. These observations are further supported by **Figure 20**, which presents numerical stress analysis, crack initiation zones, and μCT scans of failed specimens.

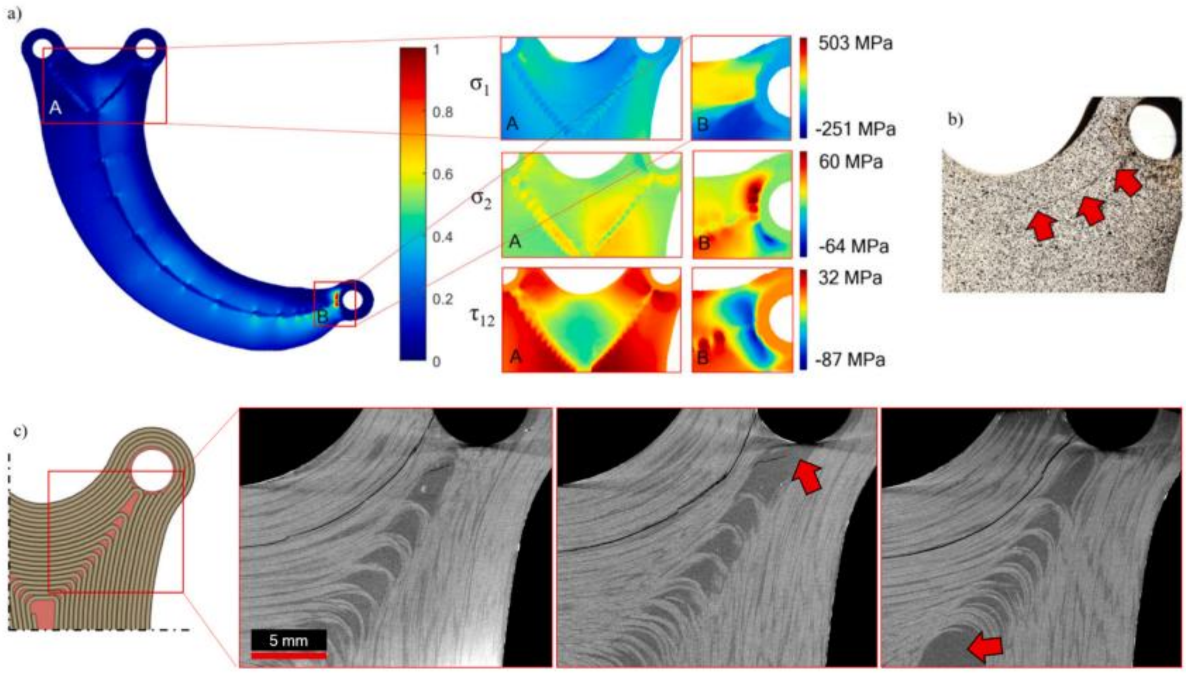

Figure 20. *(a) FEA Tsai–Wu failure contour with insets showing shear stresses. (b) Close-up of crack formation at failure. (c) μCT slices of the failed coupon compared with the corresponding close-up of the design. Adapted from [27].*

Broader reviews by Brenken et al. (2018) [74] emphasized that fiber alignment increases stiffness but reduces transverse strength, highlighting interlayer adhesion as critical. Large-scale systems, such as Big Area Additive Manufacturing (BAAM) and Large-Scale Additive Manufacturing (LSAM), improved production speeds but still face challenges in accurately predicting fiber orientation, improving interlayer bonding, and modeling residual stress. Brenken et al. (2019) [77] validated finite element models predicting residual stresses and deformation in printed composites but identified limitations in modeling layer adhesion failures, especially for large-scale parts. Tekinalp et al. (2014) [73] experimentally demonstrated high fiber alignment in carbon fiber-reinforced ABS composites, significantly enhancing mechanical performance despite increased porosity. These composites matched or exceeded aluminum alloys' specific strength, demonstrating their structural potential.

Despite these advancements, real-world applications still face major challenges such as void formation, fiber misalignment, and weak interfacial bonding. Zhang et al. (2025) [19] and Plamadiala et al. (2025) [78] reviewed common defect types and process-level strategies to mitigate them, including in situ heating and tailored deposition. However, these techniques offer only partial solutions and often require compensatory adjustments to extrusion temperature, nozzle geometry, or material formulation.

These limitations have prompted efforts to more accurately incorporate experimental imperfections into simulation models. For example, Somireddy et al. (2022) [79] developed and compared two finite element models of ABS–short carbon fiber composites, aiming to capture the effects of interfacial defects and fiber alignment. As shown in **Figure 21**, Model CM-1, based on virgin ABS properties, significantly overestimated stiffness and strength, while CM-2, which incorporated tensile data from printed specimens, more accurately reflected the nonlinear behavior observed in experiments. This comparison underscores the importance of using real defect-informed material data to improve the predictive reliability of composite FFF simulations.

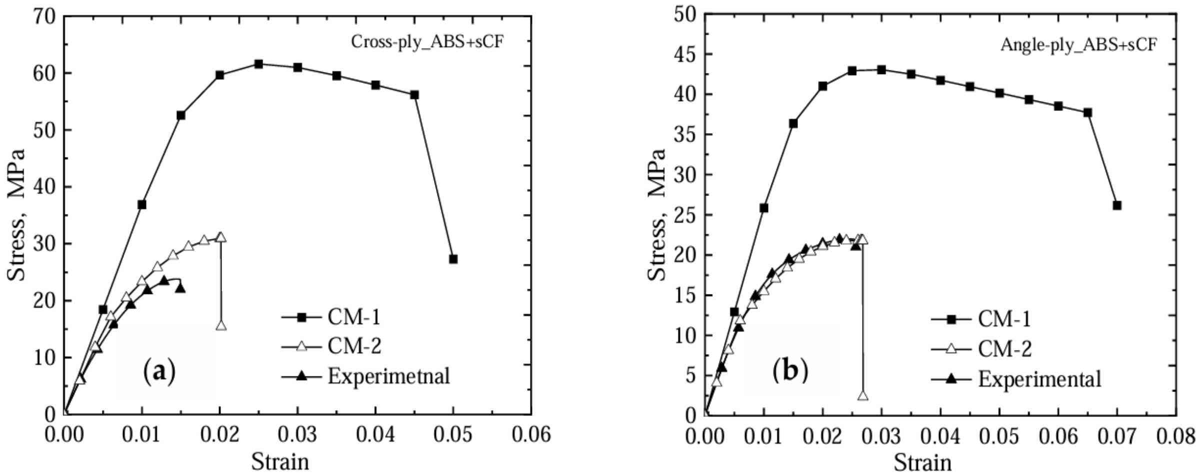

***Figure 21**. Stress–strain curves of ABS–sCF composite specimens under uniaxial tensile loading for (a) cross-ply and (b) angle-ply printing strategies, comparing computational models CM-1 and CM-2 with experimental results. Adapted with permission from [79].*

Building upon the need to better capture and control defect formation, recent studies have explored intelligent control strategies during the printing process. Lu et al. (2023) [22] developed a deep learning-assisted framework for real-time defect detection and closed-loop adjustment in the fabrication of continuous fiber-reinforced polymer composites. By integrating sensor data with neural network-based decision models, their system detected anomalies and adaptively modified print parameters to prevent defect propagation. This architecture not only improved process reliability but also demonstrated the feasibility of combining artificial intelligence with physical simulation to enhance control in fiber-reinforced FFF.

Taken together, these studies reveal both the potential and the persistent limitations of fiber-reinforced FFF. While predictive models have become increasingly sophisticated, they still struggle to fully capture the coupled effects of fiber orientation, bonding quality, and defect distribution. One of the key remaining gaps is the ability to link microstructural behavior to macroscopic performance. Recent approaches, such as thermal–mechanical models with in situ deformation tracking [80] and hybrid machine learning frameworks that incorporate physical laws [81], have begun to address this. However, progress is constrained by the lack of standardized validation methods. Moving forward, a combination of high-fidelity simulations, robust experimental datasets, and process-aware material models will be essential to bridge the gap between theory and application in composite FFF.

2.5. Systematic Literature Review

Numerical modeling of FFF with PLA has been implemented using a range of simulation tools capable of capturing thermal, mechanical, and rheological behavior during deposition, as discussed in previous sections. Common platforms include Ansys, Abaqus, COMSOL [82], UMFPACK [12], Slic3r [11], multi-scale algorithms [83], and custom in-house models [84]. The following section presents a focused comparison between Ansys and Abaqus, given their extensive application and advanced finite element capabilities in FFF modeling.

2.5.1. Comparative Evaluation of Abaqus and Ansys

Abaqus has been widely used to simulate the mechanical behavior of FFF-processed PLA, particularly through implementations that support advanced thermo-mechanical modeling. Favaloro et al. (2017) [85] explored recent functionalities in Abaqus, based on the sequentially coupled thermo-mechanical approach developed by Brenken (2017) [86], incorporating UMAT subroutines to define material behavior. In a separate study, [14] performed detailed mesoscopic and macroscopic simulations of the FFF process using Abaqus. Talagani et al. (2015) [87] modeled the additive manufacturing of a full-scale vehicle with Abaqus and GENOA, where GENOA automatically generated a structured mesh based on G-code tool paths.

Abaqus has proven effective in modeling the tensile, compressive, and flexural testing of PLA specimens using FEA [84], [88], [89], [90], [91], [92], [93], [94]. Across the reviewed studies, the integration of subroutine codes, often based on G-code, has contributed to robust mechanical representations of PLA parts [87], [91]. Ansys has also demonstrated significant capability in simulating the FFF process. Zhang and Chou (2006) [95] developed a model incorporating heat and mass transfer, mechanical loading, and phase change using element activation within Ansys, enabling the simulation of residual stresses and part distortion. They assumed complete contact between deposited layers and the substrate, simplifying the representation of bead interfaces. In a follow-up study, Zhang and Chou (2008) [96] examined how variations in printing parameters influence distortion through sequentially coupled thermo-mechanical simulations.

Expanding on this approach, Xu et al. [97] presented a non-isothermal viscoelastic fluid dynamics model using Ansys Fluent to analyze the effects of transient and constant feeding forces, phase transitions, and the viscoelastic behavior of semi-crystalline polymers. These simulations addressed flow behavior, heat transfer, and structural responses using finite volume methods. In addition to thermo-mechanical analysis, Ansys has supported the modeling of PLA's rheological properties [98], [99], [100], [101], [102] via the Fluent module and mechanical characterization using its Solid module [98], [99], [100], [101], [103], [104], [105]. These studies explored material behavior under various loading and processing conditions, including melt flow, fracture growth, shear stress, and the optimization of extrusion parameters.

The comparative analysis of Abaqus and Ansys also involves practical criteria such as potentiality, usability, scalability, and accessibility (**Table 1**). Ansys offers specific modules for additive manufacturing, such as Additive Print and Additive Suite, which streamline simulation setup for metallic and polymeric materials. Its integration with Fluent provides comprehensive support for CFD and thermo-mechanical problems. Abaqus, on the other hand, offers extensive flexibility through subroutines such as UMAT and VUMAT, and is frequently chosen for tasks requiring customized material definitions and process control. In terms of file compatibility, both platforms support a wide range of import and export formats. Ansys accepts formats such as .igs, .step, .stl, .txt, .csv, .inp, .xml, .dat, and Fluent-specific formats (.cas, .dat). Abaqus supports .sim, .prt, .mdl, .cdb, .eaf, .cfx, .CATPart, .CATProduct, .igs, .nas, .bulk, .x_t, .stp, .step, and .wrl, among others. Abaqus also demonstrates better integration with SolidWorks and CATIA, which are common in industry environments. Programming environments differ as well. Abaqus primarily uses Python for scripting and automation and Fortran for user-defined subroutines (e.g., UMAT, VUMAT, USDFLD). Ansys relies on APDL for parametric modeling and provides Python support through its Workbench environment and ACT extension. Although APDL is powerful, users generally report greater accessibility with Abaqus's Python-based scripting.

Both platforms are scalable and well-suited to mechanical testing applications. Ansys is particularly strong in CFD applications due to Fluent, which supports simulations involving fluid flow, heat and mass transfer, and complex physical reactions with high fidelity. Abaqus offers similarly robust mechanical modeling tools, especially for studies requiring precise sub-routine integration. Access to both platforms is facilitated through academic versions, although these are limited in computational capacity and customization options. Licensing structures are comparable, with Ansys often sold in modular packages and Abaqus in bundled configurations. Both companies provide broad documentation, international support, professional certification, and training programs for various user levels.

Table 1. *Software comparison based on specific criteria.*

Software/Criteria	Potentiality	Usability	Scalability	Accessibility
Abaqus	High	Very high	High	High
Ansys	Very high	High	Very high	High

2.6. Discussion and Future Trends

The evolution of numerical simulations in FFF has significantly advanced the understanding of material flow, thermal effects, and mechanical behavior, leading to better process control and part optimization. However, challenges remain, particularly in accurately predicting material behavior, improving real-time detection, and optimizing fiber reinforcement strategies. While computational models and experimental studies have enhanced our knowledge of extrusion stability, interlayer adhesion, and residual stress formation, gaps persist in multi-scale modeling, process standardization, and large-scale industrial implementation.

One of the primary limitations in melt flow modeling is the incomplete integration of pseudoplastic and viscoelastic effects, polymer shrinkage, and multi-phase interactions in numerical simulations. Current CFD studies have refined predictions of filament shape evolution and deposition flow, but they often assume Newtonian or isothermal conditions, failing to capture non-Newtonian shear-thinning behavior in thermoplastics [65]. Future research should focus on advanced multi-phase CFD models that couple thermal, rheological, and viscoelastic properties, enabling higher-fidelity extrusion simulations that align with experimental results. Additionally, the impact of high-speed extrusion on melt behavior remains underexplored, requiring models that incorporate shear stress-induced polymer degradation and flow instabilities under rapid deposition conditions [46].

The cooling and solidification phase is another field requiring further study, particularly regarding heat transfer mechanisms, interlayer diffusion, and generated residual stresses. While previous studies have confirmed that controlled chamber environments and print bed heating reduce residual stress and warping [63], there is a lack of standardized thermal models that account for material-dependent cooling rates and anisotropic heat conduction in fiber-reinforced composites. Future studies should integrate thermo-mechanical models with in situ temperature monitoring to predict real-time stress evolution during the printing process. Additionally, research should focus on adaptive cooling strategies, such as localized heat control near the extrusion zone, to prevent premature solidification and adhesion defects [56].

The thermo-mechanical behavior of FFF-printed components is significantly affected by deposition-induced residual stresses, temperature gradients, and the anisotropy arising from the layer-by-layer manufacturing process. Although coupled CFD–FEA models have improved predictions of deformation and internal stress distribution, many simulations lack material-specific calibration, particularly for biocomposites and high-performance polymers [67]. Future research should focus on multi-scale simulation frameworks that integrate real-time temperature tracking, stress relaxation mechanisms, and phase transitions to improve stress accumulation modeling. Moreover, increased efforts toward developing standardized validation protocols will be crucial to bridging the gap between simulations and experimental reality, ensuring that numerical models provide reliable predictions for industrial applications.

The characterization of material properties in FFF presents additional challenges due to anisotropic behavior, microstructural defects, and complex fiber–polymer interactions. While previous studies have validated the effect of building orientation, raster angle, and layer thickness on mechanical strength, existing models often overestimate failure strength by neglecting interfacial bonding imperfections [15], [70]. Future studies should focus on hybrid experimental–numerical approaches, where high-fidelity microstructural imaging (X-ray µCT, SEM) is integrated with simulation-based failure predictions to refine fracture and deformation models. Another critical research direction involves fiber-reinforced composites, where current models fail to fully capture fiber breakage, alignment errors, and void formation [73], [74]. More advanced multi-scale fiber orientation models should be developed to predict fiber motion during deposition, ensuring optimized mechanical properties and structural integrity.

For fiber-reinforced composites, while CFRCs have demonstrated exceptional mechanical performance, they introduce manufacturing challenges related to fiber placement, matrix bonding, and deposition precision. Current topology optimization frameworks have improved load distribution and material efficiency, but they remain limited by fiber misalignment during printing [27], [76]. Future research should develop automated path-planning algorithms that adaptively adjust fiber orientation based on in situ stress distribution data. Additionally, real-time reinforcement monitoring using AI-driven vision systems could improve defect detection in large-scale composite printing [21]. Lastly, large-scale applications in aerospace and automotive manufacturing require further investigation into void formation, pressure fluctuations, and thermal expansion effects in Large Area Additive Manufacturing (LAAM). While models have been developed to predict fiber-induced pressure variations and flow disturbances, they require more accurate fiber-matrix interaction models [29]. Future work should integrate non-Newtonian flow effects and high-resolution fiber–resin interface simulations to improve prediction accuracy for industrial applications.

2.7. Conclusions

FFF has become a widely used additive manufacturing technology, but challenges remain in simulation accuracy, material performance, validation, and process optimization. Advances in CFD and FEA models have improved predictions of melt flow, cooling behavior, and stress accumulation, while fiber-reinforced composites enhance mechanical properties but require further refinement in extrusion, bonding control, and fiber-matrix interactions. The lack of standardized experimental validation limits the accuracy of numerical models, reinforcing the need for universal testing protocols to ensure reproducibility and alignment between simulated and real-world performance. The choice of simulation software also plays a critical role in this context: Abaqus offers advantages in mechanical characterization and model customization via G-code or user subroutines, while Ansys is better suited for multiphysics and rheological simulations, particularly when model integration and fluid-structure interactions are required. Future research should focus on hybrid simulation frameworks that combine physics-based models with real-time sensor feedback, the use of machine learning for defect detection and adaptive control, and the development of robust validation benchmarks to support model generalization across materials and process conditions.

Chapter 3

Experimental and Numerical Assessment of FFF-Printed PLA: A Comparative Study Using Optical Strain Techniques [2]

Abstract: Fused Filament Fabrication (FFF) enables the production of complex polymer components with high geometric freedom and minimal material waste. Among thermoplastics, polylactic acid (PLA) remains a preferred material due to its biodegradability and ease of printing. However, its mechanical behavior is highly sensitive to process-induced anisotropy, which challenges experimental repeatability and numerical modeling. This study presents a comparative assessment of two non-contact optical strain measurement techniques, Digital Video Extensometer (DVE) and Two-Dimensional Digital Image Correlation (2D-DIC), applied to tensile testing of FFF-printed PLA specimens. Finite Element Analysis (FEA) is used to simulate the elastic response under standardized boundary conditions, with results validated against the most representative experimental dataset. While DVE provided consistent stress–strain curves and measurable yield behavior in select samples, DIC revealed limitations in tracking full-field deformation up to failure. The numerical model, based on linear elasticity, accurately reproduced experimental stiffness and stress distribution in the most structurally coherent specimen. The findings highlight the influence of manufacturing variability on test outcomes and underscore the need for improved specimen consistency and refined strain acquisition protocols to support reliable experimental–numerical correlation in FFF research.

Keywords: Digital Video Extensometer (DVE); Digital Image Correlation (DIC); Finite Element Analysis (FEA).

[2] Enriconi, M. et al., 2025. Experimental and Numerical Assessment of FFF-Printed PLA: A Comparative Study Using Optical Strain Techniques. Manuscript preparation for submission a scientific journal.

3.1. Introduction

FFF has emerged as one of the most widely adopted AM technologies for producing thermoplastic components, offering advantages such as geometric flexibility, low cost, and reduced material waste [10], [89]. However, the mechanical performance of FFF-printed parts, especially those made from PLA, remains inconsistent due to the combined influence of processing parameters and thermal history.

To investigate these dependencies, the present study integrates numerical and experimental approaches to characterize the elastic behavior of FFF-printed PLA specimens. A two-fold numerical framework was developed: first, a transient thermal simulation was conducted using the DED module in ANSYS Workbench to reproduce the heat transfer dynamics during material deposition. This model employs an element birth-and-death strategy driven by G-code data, enabling the analysis of thermal gradients, cooling profiles, and interlayer temperature evolution. Such simulations are useful to identify potential sources of anisotropy and bonding irregularities and have been successfully applied in polymeric and composite systems [14], [23].

In parallel, a finite element model was implemented to simulate tensile loading under idealized conditions replicating the boundary constraints applied during physical testing. The model assumes linear elastic behavior and incorporates experimental dimensions and constraints to reproduce the stress-strain response of printed PLA specimens. This mechanical simulation serves as a reference to interpret the experimental data and assessing the spatial distribution of deformation.

PLA is a bio-based, biodegradable polymer known for its ease of printing, but it exhibits brittle behavior and significant variability in mechanical performance when processed via FFF [24], [25]. These variations are strongly influenced by factors such as print orientation, filament quality, layer adhesion, and local thermal conditions during deposition [16], [106]. Even when standardized specimen geometries and protocols are followed, such as ISO 527-1, variations in porosity, thickness, and fracture location can undermine repeatability [7], [17].

To experimentally characterize the elastic response and support model validation, tensile tests were performed using non-contact optical techniques. DVE and 2D-DIC were employed to capture pointwise and full-field strain measurements, respectively. These methods are particularly suitable for testing brittle polymers prone to premature or asymmetric fracture, where traditional contact extensometers may be unreliable [15], [16].

The study also addresses critical factors such as fabrication quality, optical tracking limitations, and normative compliance, all of which influence both the accuracy of experimental results and the predictive reliability of numerical simulations. By combining thermal and mechanical simulations with high-resolution experimental measurements, this methodology provides a structured basis for future integration of more advanced analyses, such as the prediction and validation of residual stress fields, in FFF-printed PLA components.

3.2. Material and Methods

3.2.1. Raw Material

The material used in this study was Ingeo 4043D PLA, a commercial-grade biodegradable thermoplastic from NatureWorks LLC (USA). It was employed in both the experimental tests and the numerical simulations. The material model in ANSYS was defined using a combination of datasheet values and experimental data: density, tensile yield strength, and ultimate strength were taken from the Ingeo 4043D technical datasheet, while melting temperature and Young's modulus were obtained from experimental results. **Table 2** summarizes the properties used and their respective sources.

Table 2*. Material properties of PLA (ANSYS vs. Ingeo 4043D).*

Property	ANSYS	Ingeo 4043D
Density [Kg/m³]	Ingeo	1240
Melting Temperature [ºC]	Ingeo	160
Young's Modulus [GPa]	Ingeo	3,6
Tensile Ultimate Strength [MPa]	Ingeo	60
Tensile Yield Strength [MPa]	Experimental	-

Although minor numerical differences are observed between sources, all values fall within accepted ranges for standard-grade PLA. The datasets were deemed sufficiently representative to support the comparative approach adopted between experimental and simulation-based analyses.

3.2.2. Numerical Modeling and Simulation

Numerical modeling was employed in this work to characterize both the thermal behavior during the additive manufacturing process and the mechanical response of FFF-printed PLA specimens under uniaxial loading. Two independent yet complementary simulations were developed using ANSYS Workbench 2024 R2: one aimed at replicating the thermal evolution during deposition, based on the Directed Energy Deposition (DED) process via the AM module, and the other focused on the elastic response of the part during tensile testing, modeled in the Static Structural environment.

In both simulation workflows, the geometry was derived from the standard ISO 527-1 Type 1A tensile specimen (**Figure 22**). The nominal dimensions were total length of 170 mm (l_3), width of 10 mm (b_1), and thickness of 4 mm (h). A detailed 3D CAD model was created and exported in STL format, then imported into ANSYS. As is typical for STL files, the geometry was initially interpreted as a faceted surface composed of triangular elements. To enable accurate mesh generation and compatibility with solver tools, the model was converted into a solid body using ANSYS SpaceClaim, as shown in **Figure 23**. This step ensured numerical stability and allowed the use of structured meshing strategies required by both simulation environments.

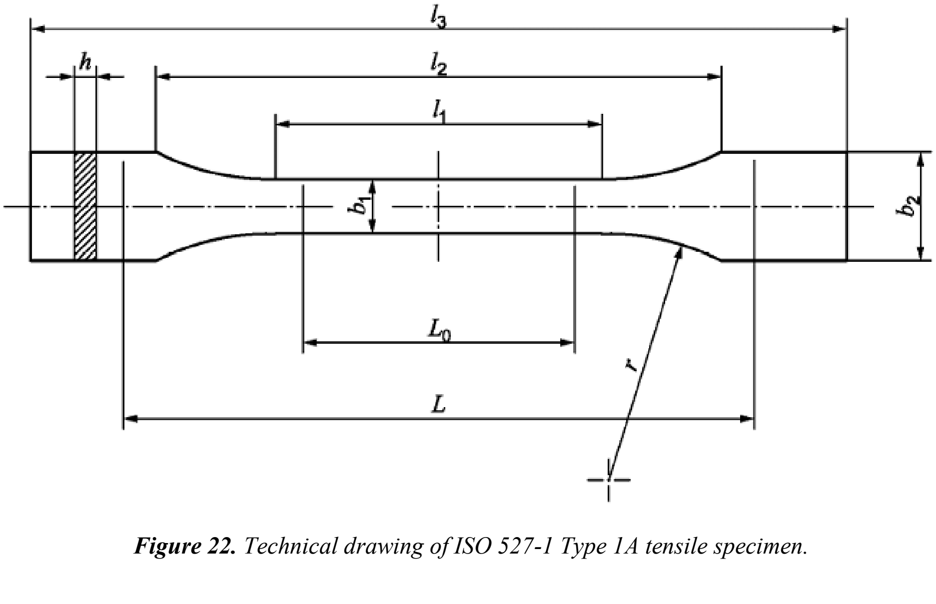

Figure 22. *Technical drawing of ISO 527-1 Type 1A tensile specimen.*

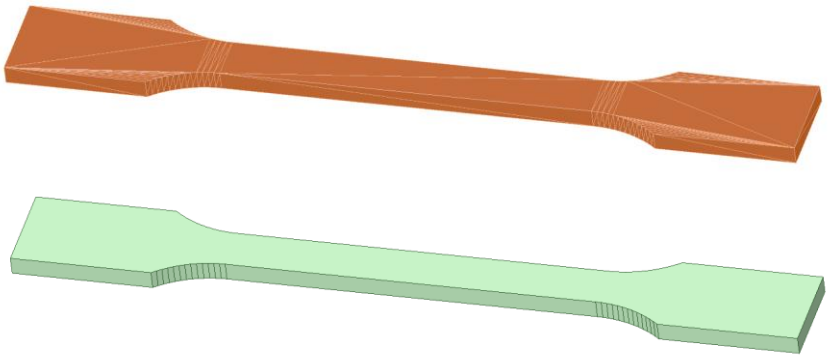

Figure 23. *Conversion of STL mesh to solid geometry using ANSYS SpaceClaim.*

A mesh convergence analysis was carried out for both simulations (**Figure 24**). Element sizes ranging from 6 mm to 1 mm were tested, and a resolution of 2 mm was identified as optimal, at which point the results stabilized with negligible variation. This element size was adopted in both models to provide a good balance between numerical accuracy and computational efficiency.

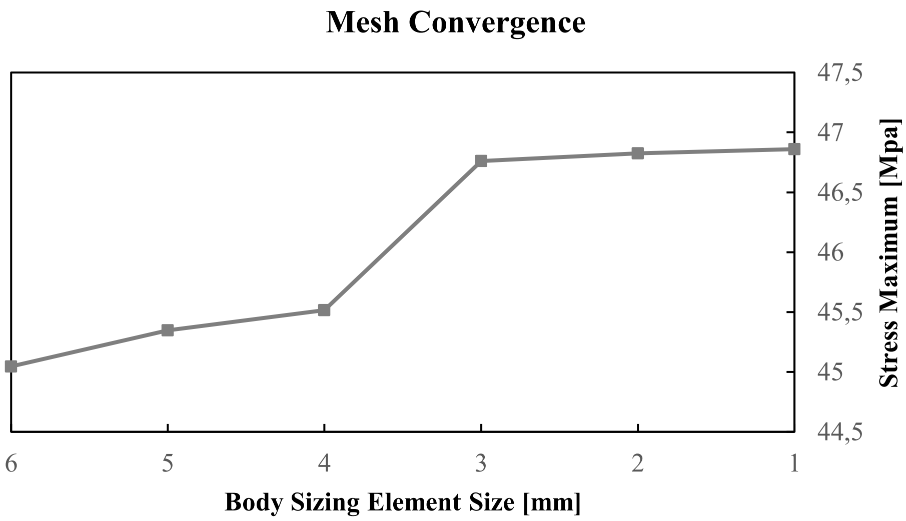

Figure 244. *Mesh convergence analysis: maximum stress variation with decreasing element size.*

3.2.3. Thermal Simulation of PLA Deposition

The thermal simulation of the printing process was performed using the DED Process available in the Additive Manufacturing module of ANSYS Workbench 2024 R2. This tool provides a step-by-step interface to define build geometry, mesh settings, material properties, weld path, and thermal boundary conditions. The simulation follows a transient thermal approach, based on the element birth and death method, in which the entire geometry is meshed at once and individual element clusters are sequentially activated to replicate the progressive deposition of material.

The mesh used body-fitted Cartesian elements with a target element size of 2 mm, as defined by the convergence analysis. The deposition path was generated from a G-code file containing the machine instructions for the actual print, including tool movements and layer definitions (**Figure 25**). The DED wizard parsed this file to define the build order and cluster activation sequence. Clustering was used to divide the weld paths into element groups, which were progressively activated to simulate heat input along the deposition path.

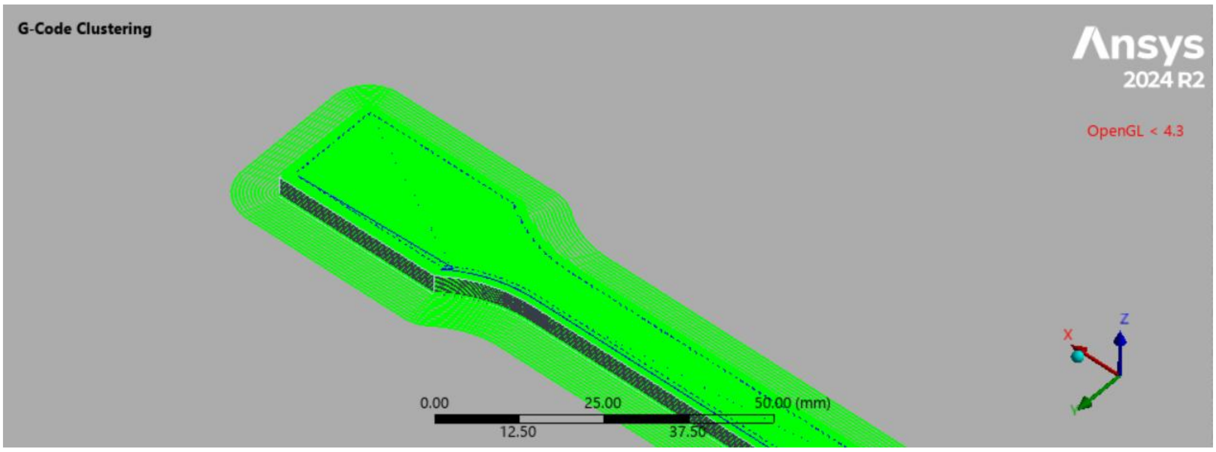

Figure 25. *Clustering of G-code-based deposition paths for progressive activation in the DED simulation.*

The simulation adopted a temperature-based heating method, where each activated cluster was exposed to a defined process temperature corresponding to the molten state of PLA. The process temperature was set to 160 °C, matching the PLA melting point. The base plate was initialized with a preheat temperature of 60 °C to reflect typical starting conditions. Heat transfer during the process was driven by the sequential cluster activation. After completing the wizard steps and performing the clustering procedure, the simulation was executed as a transient thermal analysis. The results enabled the evaluation of heat propagation, cooling gradients, and temporal thermal profiles during the simulated build. Key simulation parameters used in this stage are summarized in **Table 3**.

Table 3. *Thermal build conditions applied in the simulation.*

Parameter	Value	Unit
Material Deposition Rate	45	mm^3/s
Preheat Temperature	60	ºC
Process Temperature	160	ºC

3.2.4. Structural Simulation of the Tensile Test

The structural simulation was designed to evaluate the uniaxial elastic behavior of the PLA tensile specimen based on the same geometry used in the thermal simulation and the actual printed parts. The mesh used in this model followed the convergence study described in Section 3.2.2, adopting a uniform element size of 2 mm to ensure accuracy and computational efficiency. Displacement boundary conditions were applied only to one end of the specimen in the X-direction (**Figure 26**), using a time-dependent linear function that replicated a loading rate of 2 mm/min:

$$Displacement = 0.033 \times time$$

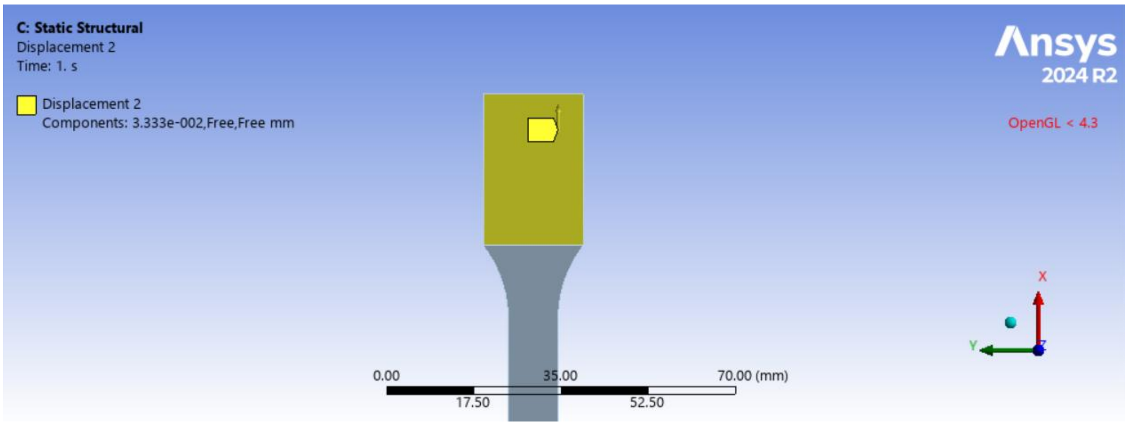

Figure 26. *Displacement boundary condition applied at the top surface to simulate the loading point.*

The opposite end of the specimen was fully constrained, with all translational degrees of freedom (X, Y, and Z) fixed to simulate the clamped condition of the test fixture (**Figure 27**). This configuration ensured that deformation occurred along the X-axis only, under controlled uniaxial loading.

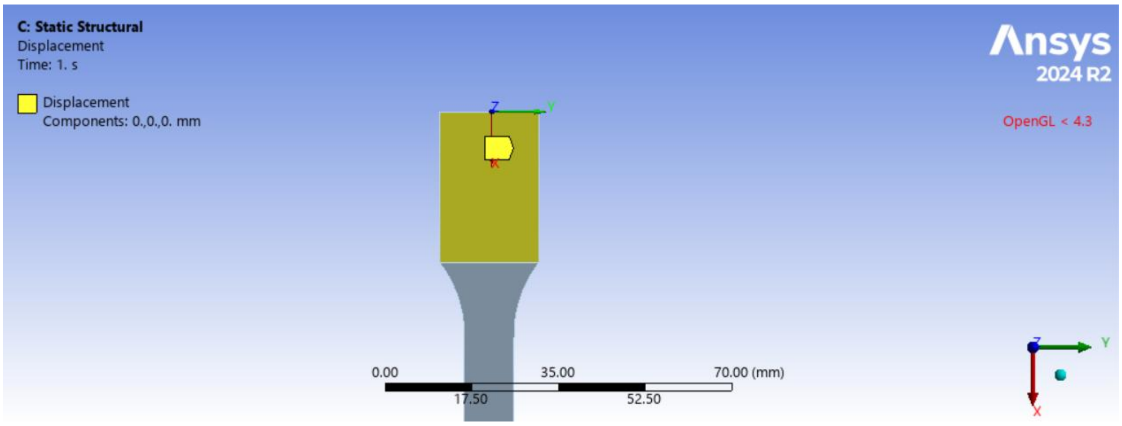

Figure 27. *Boundary condition applied at the bottom surface, constraining translations in the X, Y, and Z directions.*

The simulation was conducted under small deformation assumptions, with geometric nonlinearity and contact effects disabled, focusing solely on the elastic regime of the material.

3.2.5. Fabrication of Tensile Test Specimens

Specimen fabrication followed the recommendations outlined in ISO 527-1 and ISO 527-2, which define the geometry, mechanical test conditions, and reporting standards for polymeric materials. To ensure reproducibility and minimize the impact of moisture on melt flow and interlayer adhesion, PLA pellets were first dried in a convection oven at 80 °C for 20 hours. The dried PLA pellets were extruded into filament using a 3devo Composer 350 single-screw extruder, operating with a four-zone heating profile (170 °C – 185 °C – 190 °C – 170 °C) and a constant screw speed (3.5 rpm). Cooling was carried out via ambient airflow, and a laser diameter measurement system ensured that the filament diameter remained within 2.85 mm ± 0.10 mm, providing dimensional consistency for the subsequent printing process.

Tensile specimens were designed according to the Type 1A geometry specified by ISO 527-1. The CAD model was exported in STL format and processed with Ultimaker Cura for slicing (**Figure 28**). Key slicing parameters included: 100% grid infill, 0.5 mm layer height, 1.5 mm line width, 1.5 mm wall thickness, and 2 mm top and bottom layers. Retraction settings were defined as 4 mm distance, 100 mm/s speed, and 0.5 mm Z-hop, with fan cooling set to 100% for thermal consistency during deposition.

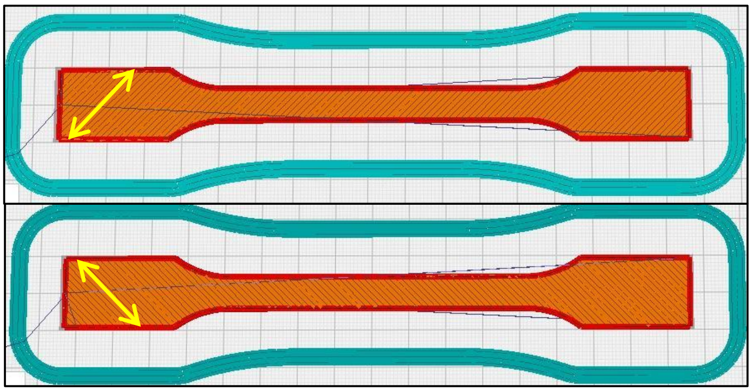

Figure 28. *Slicing preview of the tensile specimen in Ultimaker Cura, showing layer deposition path.*

Printing was carried out on a custom-built FFF 3D printer (**Figure 29**), configured with a nozzle temperature of 210 °C, a heated bed at 60 °C, and a print speed of 60 mm/s. Specimens were printed flat, with their longitudinal axis aligned with the printer's X-direction, resulting in an XY build orientation as defined in ISO 17295 and ISO/ASTM 52924:2024. This orientation was deliberately chosen to align the tensile axis with the direction of maximum interlayer continuity, improving structural coherence in the printed parts.

Figure 29. *Custom-built FFF 3D printer used for printing PLA tensile specimens.*

The fabrication process was divided into two distinct filament production batches. One batch was used for specimens tested with DVE, and the other for 2D-DIC. Although both batches were fabricated using identical extrusion and printing parameters, slight dimensional and mechanical variations were observed between them, likely due to inter-batch differences in filament quality. These variations are discussed later in the results and analysis sections. Each group consisted of eight specimens.

3.2.6. Tensile Testing Using a Digital Video Extensometer

Mechanical testing of the first specimen group was conducted using a Servosis ME 405-1 universal testing machine, operated under displacement control with a fixed crosshead speed of 2 mm/min, in compliance with the procedures defined in ISO 527-1 for thermoplastic materials. The strain measurement system employed was the X-Sight 4101-D DVE, which was fully integrated with the machine's data acquisition interface. The optical configuration included a fixed camera and lighting arrangement, calibrated to maintain image contrast, and reduce tracking errors caused by specimen deformation. The complete setup is in **Figure 30**.

Figure 30. *DVE setup (X-Sight 4101-D) integrated with the Servosis ME 405-1 and lighting arrangement.*

To enable reliable displacement tracking, each specimen was manually prepared with a high-contrast speckle pattern applied to the gauge section. A uniform matte white paint base was first applied to the surface, followed by a random distribution of black speckles generated via aerosol spray from a controlled distance. This dual-layer approach provided the optical texture necessary for feature recognition within the extensometer's software environment (**Figure 31**).

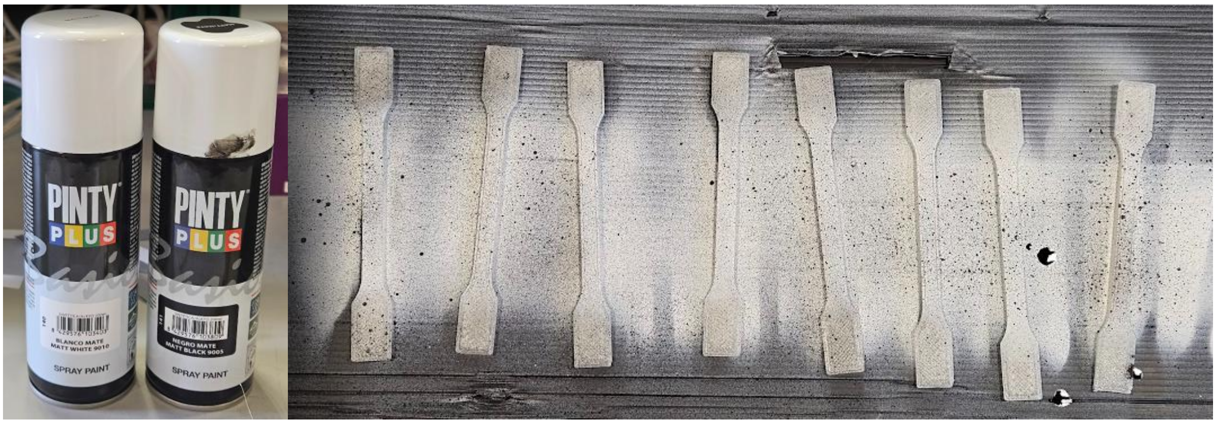

Figure 31. *High-contrast speckle pattern manually applied to the gauge section using white and black spray paint.*

Each specimen was carefully mounted between mechanical grips, ensuring axial alignment to avoid eccentric loading or lateral bending. Clamping force was applied uniformly to both ends. Once secured, six virtual extensometers were defined along the longitudinal axis of the gauge region using the X-Sight software interface. These tracked point-to-point displacements between fixed regions of interest as the load progressed (**Figure 32**).

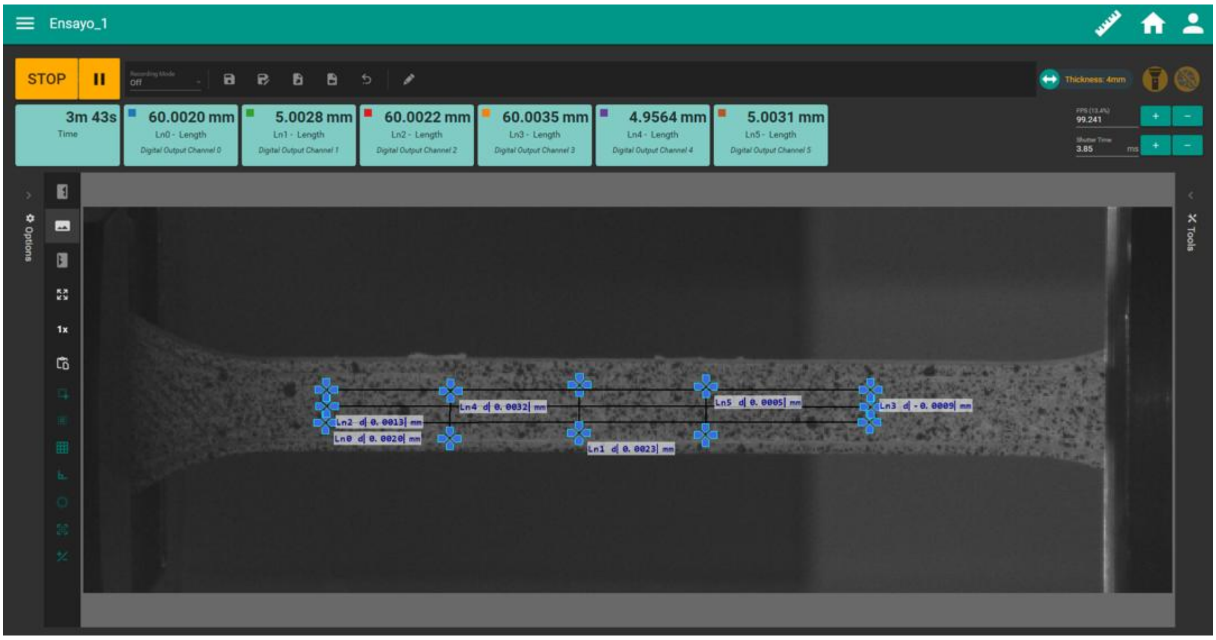

Figure 32. *Virtual extensometers are defined on the speckled specimen surface using the X-Sight software interface.*

During testing, data were acquired at a frequency of 99 Hz, with a shutter exposure time of 3.85 ms, allowing for the capture of micrometric displacements with high temporal fidelity. The software interface displayed synchronized numerical outputs and real-time force–displacement curves, enabling the monitoring of specimen behavior throughout each test.

3.2.7. Tensile Testing Using Two-Dimensional Digital Image Correlation

The second group of specimens was subjected to tensile testing using 2D-DIC, a full-field optical technique for measuring surface strain. Testing was performed on a Servosis ME-405/50/5 universal testing machine, equipped with a TC50kN REP load cell and MTS XSA304A mechanical grips. The same crosshead displacement speed of 2 mm/min was maintained, ensuring parity with the DVE setup.

Image acquisition was carried out using a Canon EOS 700D DSLR camera mounted on a rigid optical rail. The camera was fitted with a 60 mm macro lens and featured an APS-C CMOS sensor with a resolution of 5184 × 3456 pixels, a pixel size of 4.3 µm, and sensor dimensions of 22.3 × 14.9 mm. These specifications allowed for accurate detection of small-scale displacements across the specimen's surface.

The camera was aligned orthogonally to the plane of the specimen using a micrometric ball joint and a digital inclinometer to eliminate parallax errors. Lighting was provided by two high-intensity LED floodlights positioned symmetrically on either side of the gauge region. The optical setup and camera configuration are presented in **Figure 33a**. Image and mechanical data synchronization was achieved using a Siemens LOGO programmable logic controller (PLC), which triggered both the camera and the HBM QuantumX acquisition system. Each image capture event was registered by a 100 V digital pulse, recorded on an auxiliary channel, thereby enabling precise time alignment between visual frames and force data (**Figure 33b**).

(a) (b)

Figure 33. *(a). Complete DIC optical setup: DSLR camera (Canon EOS 700D) with macro lens mounted on the optical rail, lighting, and testing machine. (b). Synchronization system with Siemens PLC and HBM QuantumX acquisition hardware.*

Each specimen received a digitally generated speckle pattern, produced using custom MATLAB scripts and printed onto adhesive transfer film. This pattern consisted of non-repetitive, randomly distributed circular dots optimized for optical tracking algorithms. The film was applied to the gauge region in a standardized manner to ensure pattern consistency across all specimens (**Figure 34**). Before each test, image quality and dot contrast were verified to ensure suitable input for the correlation algorithm.

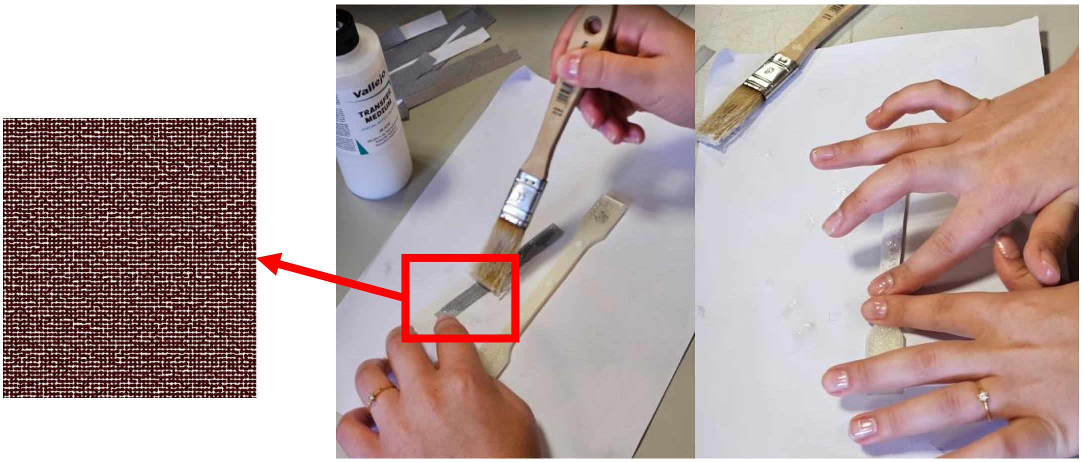

Figure 34. *Digitally generated speckle pattern applied to specimen via adhesive film.*

After mechanical testing, the captured image sequences were processed using Ncorr, an open-source MATLAB-based software package for DIC analysis. A reference image (undeformed) and corresponding deformed frames were selected, and a Region of Interest (ROI) was defined over the gauge section. This ROI was divided into square subsets, and the software computed displacement fields using normalized cross-correlation. Based on the computed fields, virtual extensometers were created along the longitudinal direction to extract local axial strain values at multiple locations within the ROI (**Figure 35**).

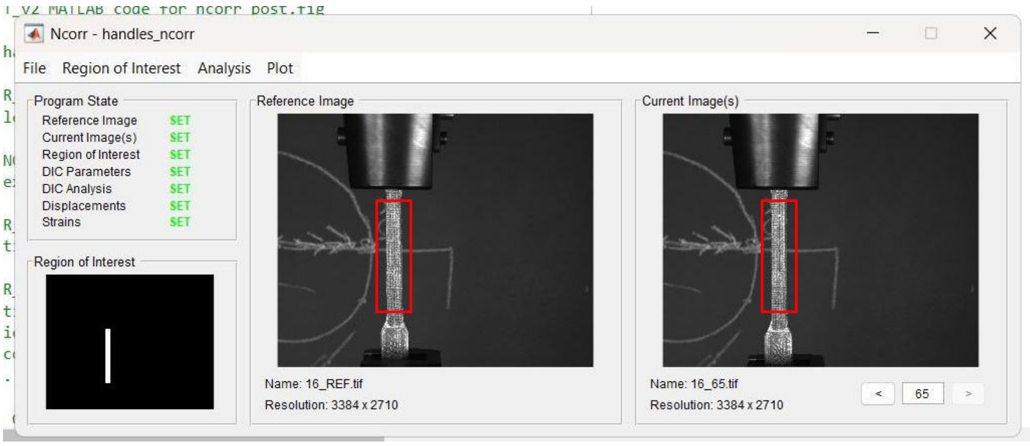

Figure 35. *Ncorr post-processing interface with region of interest and virtual extensometers.*

3.3. Results and Discussion

3.3.1. Thermal Analysis: Simulated and Experimental Results

The thermal behavior during the material deposition process was evaluated both numerically and experimentally to visualize the temperature distribution and assess the consistency between the simulated and real thermal response of the PLA material during printing.

In the simulation, the temperature field was obtained from the transient thermal analysis using the DED Process setup in ANSYS. The model captured the propagation of heat along the deposition path, with a clear temperature gradient between the active deposition zone and the surrounding cooled regions. The maximum temperature reached approximately 66 °C, and a rapid cooling behavior was observed immediately after cluster activation. **Figure 36** presents a temperature distribution map obtained during the deposition of one of the layers.

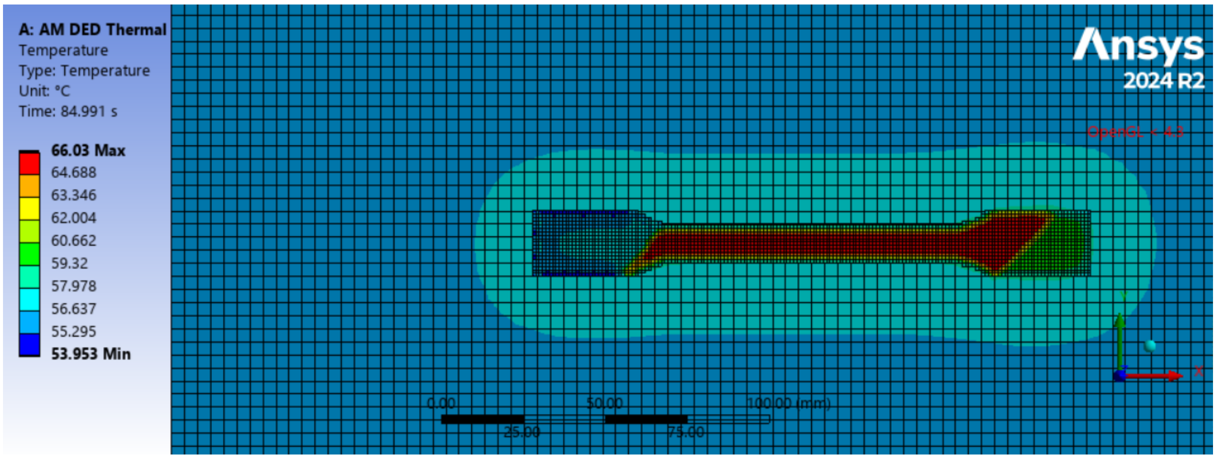

Figure 36. *Simulated temperature distribution during PLA deposition (DED model).*

To qualitatively validate the simulation, a thermal image was acquired during the real printing process using a thermal camera (Model FLIR C3). The emissivity was set to 0.95, and the image was taken approximately 30 cm from the printing bed. The recorded image shows a similar thermal pattern, with the deposition zone appearing as the hottest region, surrounded by a rapid thermal decay toward the edges of the part. This is shown in **Figure 37**.

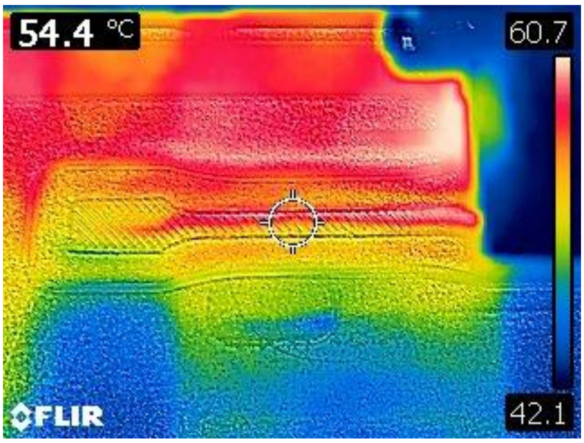

Figure 37. *Thermal image captured during the printing process using a FLIR C3.*

A visual comparison between **Figure 36** and **Figure 37** indicates that the simulation reasonably reproduces the expected thermal behavior of the process. The maximum temperature predicted by the simulation (66.03 °C) exceeded the experimental measurement (60.7 °C) by approximately 8.78%. Minor differences in intensity and gradient may result from measurement limitations, such as emissivity calibration, camera angle, and frame rate, as well as simplifications in the simulation, including uniform heat input and fixed material properties.

3.3.2. DVE Tensile Test Results

The stress–strain curves obtained from the DVE-based tensile tests are presented in **Figure 38**. The curves demonstrate clear variability in stiffness, tensile strength, and strain at failure among the eight tested PLA specimens. While specimen 8 displayed a continuous curve with identifiable yielding and post-yield behavior, most of the samples exhibited abrupt fracture following the elastic region, with little or no plastic deformation. Many curves also show an initial drop or relaxation, attributed to mechanical slack in the grips and insufficient pre-tension during test setup.

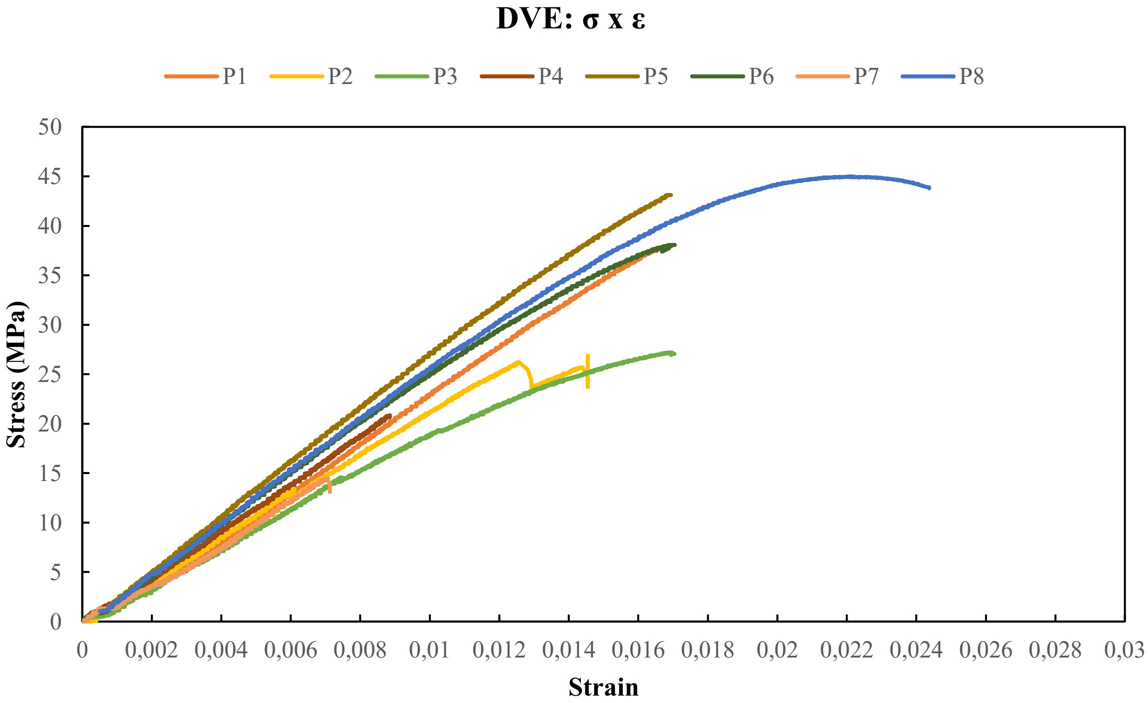

Figure 38. *Stress–strain curves obtained from tensile tests using DVE for all eight specimens.*

A summary of the mechanical performance of each specimen is shown in **Table 4**. The area was calculated individually for each specimen based on width and thickness values measured at the gauge region using a digital caliper, ensuring that stress normalization reflected the actual geometry tested. For further analysis, specimens that exhibited partial delamination of the outer wall during testing were excluded, as this defect likely compromised load transfer and strain distribution. Banjanin et al. [107] observed that PLA samples often failed outside the gauge section and exhibited larger mechanical property dispersion due to weak interlayer adhesion and air gaps. Similarly, Garg et al. [25] reported that premature failure in FFF parts often initiates at weak interlayer regions and results in stress redistribution that distorts mechanical interpretation. As a result, the mechanical parameters showed variation across samples, with the maximum deviation reaching up to 12%.

Table 4. *Mechanical properties of PLA specimens tested with DVE.*

	Area [mm²]	**Displacement [mm]**	**F max [N]**	**E [MPa]**	**σ [MPa]**
1	34,0	2,175	1279,1	2351,1	37,6
2	34,3	1,737	922,1	1887,7	26,9
3	34,4	2,031	935,3	1753,2	27,2
4	34,0	1,399	709,6	2382,1	20,8
5	32,2	1,903	1389,3	2650,8	43,1
6	33,0	2,085	1254,6	2373,2	38,1
7	34,3	1,046	495,3	2034,7	14,4
8	33,2	2,505	1491,9	2183,2	44,9
Min	32,23	1,90	1254,59	2183,20	37,64
Max	33,98	2,51	1491,92	2650,80	44,94
Mean	33,09	2,17	1353,73	2389,58	40,94
Std Dev	0,72	0,25	109,17	193,72	3,64
CV	2%	12%	8%	8%	9%

Fracture surface observations reinforce the interpretation derived from the mechanical results. As shown in **Figure 39**, specimen 8 was the only sample that fractured cleanly within the gauge section, indicating uniform stress distribution and structural continuity. Its stress-strain curve was also the only one to surpass the linear region, suggesting that the material reached and sustained plastic deformation before fracture. The curvature of the curve and the presence of a post-yield region strongly imply that this specimen approached, or potentially reached, its yield stress, a behavior not observed in the remaining samples.

In contrast, the other specimens failed near the shoulder fillet or along interlayer paths, regions associated with stress concentrations and interfacial weaknesses in FFF printing. Digital microscopy (**Figure 40**) revealed that these samples exhibited classic brittle fracture features: voids, lack of interlayer fusion, and delamination planes. Specimens 2, 3, 4 and 7 showed severe delamination that extended through the gauge cross-section, disrupting the continuity of stress transmission and leading to premature fracture. The lateral displacement measurements in these samples were likely compromised by internal failure and irregular surface movement, reflecting not true material behavior, but structural instability induced by poor interlayer bonding.

Figure 39. *Post-fracture images of representative specimens showing distinct failure locations and profiles.*

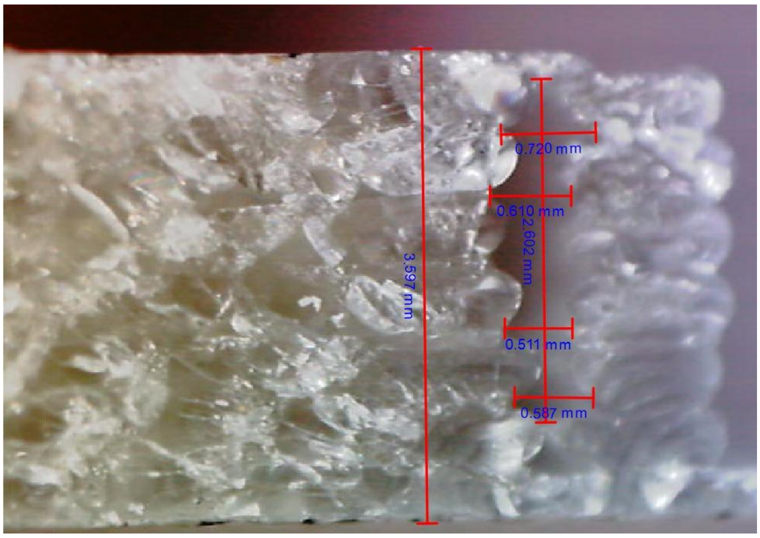

Figure 40. *Microscopic images of fracture surfaces highlighting interlayer delamination and voids (specimen 5).*

Taken together, these results confirm that the mechanical response of FFF-printed PLA is governed by the combined effects of inherent material brittleness and microstructural imperfections. As a brittle thermoplastic, PLA offers limited capacity for plastic deformation and is highly sensitive to local stress concentrators. When such defects are present, particularly poor interlayer adhesion, fracture initiates and propagates abruptly. The comparative performance of specimen 8, however, suggests that with optimal adhesion and uniform layer deposition, PLA can approach its theoretical mechanical potential, even allowing for measurable plasticity under uniaxial stress.

3.3.3. DIC Tensile Test Results

Tensile testing using 2D-DIC was performed on a second set of eight PLA specimens. The goal was to obtain full-field strain measurements across the gauge region using synchronized image acquisition and load tracking. However, several challenges emerged during testing that limited the quality and completeness of the data. Premature fracture frequently occurs outside or near the boundary of the ROI defined by the camera field of view. In line with earlier findings by [25], [107], this behavior highlights the inherent variability in PLA parts fabricated via FFF, often linked to defects such as weak interlayer bonding, porosity, and geometric inconsistencies. These factors introduce scatter in mechanical performance and complicate precise strain measurement, especially when combined with experimental issues such as loss of speckle contrast, minor defocusing, and out-of-plane displacements, common near the transition fillets. Although full tracking until failure was not achieved in any of the specimens, partial strain data were successfully extracted from the early stages of loading, before crack initiation or out-of-plane displacement compromised correlation. Virtual extensometers were placed along the gauge region using the Ncorr post-processing interface, and axial strain was evaluated up to the point where image quality or specimen behavior disrupted accurate tracking. Representative stress–strain curves obtained from this early-stage data are shown in **Figure 41**.

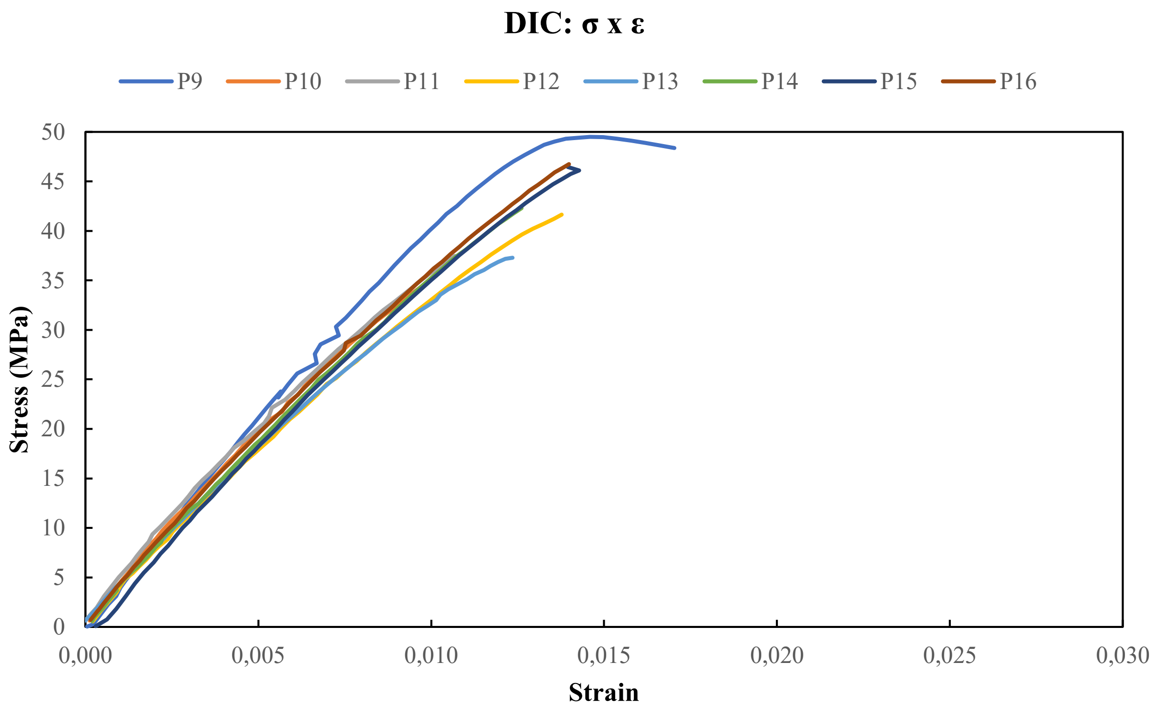

Figure 41. *Representative stress–strain curves obtained via DIC from virtual extensometers within the Region of Interest.*

The mechanical results obtained from these partial measurements are summarized in **Table 5**, while the post-fracture condition of all specimens is shown in **Figure 42**, which presents the final geometry of each sample. Although tensile strength and strain at failure could not be determined, the secant modulus (E) was reliably calculated for specimens that retained sufficient correlation during elastic loading. Notably, the coefficient of variation for E was lower than that observed in the DVE-tested group, indicating improved consistency in stiffness across this second batch of specimens. This enhancement in repeatability is likely attributable to the Z-axis calibration of the 3D printer, performed prior to the fabrication of this group. As a result, specimens exhibited greater dimensional accuracy, with thicknesses closer to the nominal 4 mm. In contrast, the first batch suffered from systematic under-extrusion, yielding thicknesses around 3.5 mm and contributing to increased dimensional variability and cross-sectional inconsistencies observed in earlier tests. Still, microscopic inspection of selected DIC-tested specimens (**Figure 43**) revealed internal voids, indicating that subsurface defects may have also played a role in the irregular strain distribution observed in some cases.

Table 5. *Mechanical properties of PLA specimens tested with DIC.*

	Area [mm²]	**Displacement [mm]**	**F max [N]**	**E [MPa]**	**σ [MPa]**
9	40,17	2,50	1988,28	3316,3	49,5
10	40,63	1,67	1440,47	3463,0	35,5
11	40,48	1,73	1516,77	3426,3	37,5
12	40,82	1,85	1725,82	3019,1	41,6
13	41,25	1,78	1538,13	3028,5	37,3
14	41,02	2,26	1734,98	3388,7	42,3
15	40,38	1,96	1866,21	3352,2	46,5
16	40,51	2,14	1893,67	3347,0	46,7
Min	40,17	1,67	1440,47	3019,10	35,45
Max	41,25	2,50	1988,28	3463,00	49,50
Mean	40,66	1,99	1713,04	3292,64	42,11
Std Dev	0,35	0,29	198,53	172,28	5,13
CV	0,9%	14,7%	11,6%	5,2%	12,2%

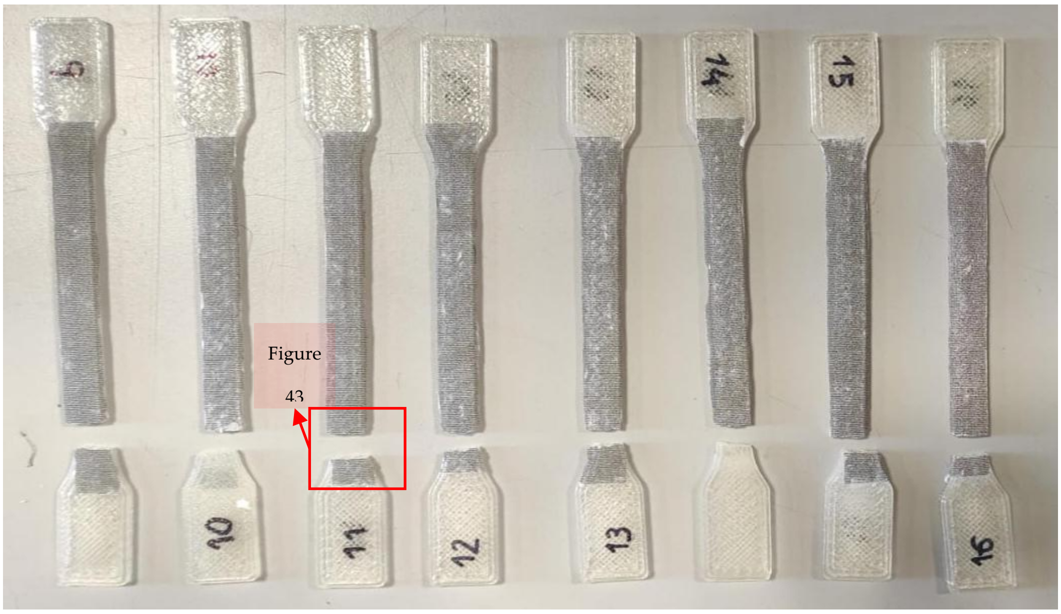

Figure 42. *Final condition of DIC specimens (9–16) after tensile testing.*

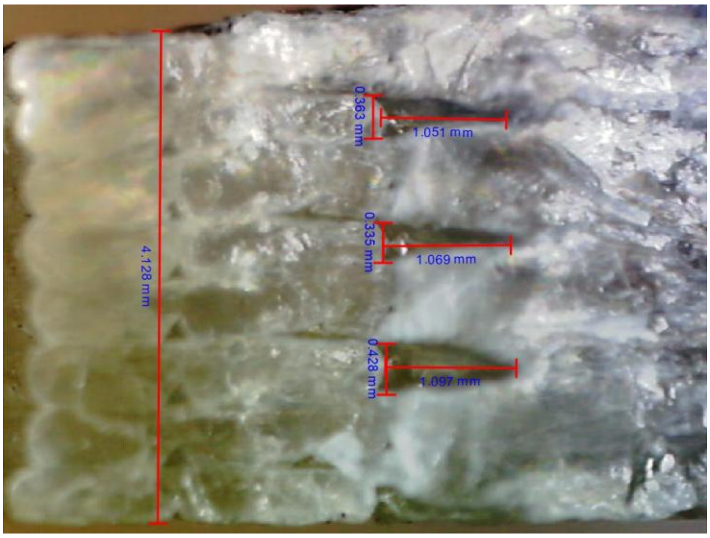

Figure 43. *Microscopic images of fracture surfaces highlighting interlayer delamination and voids (specimen 11).*

Despite the limited mechanical output, the DIC technique enabled spatial visualization of axial strain fields during the elastic loading phase. The images in **Figure 44** correspond to the initial and final physical frames of the test, with the first image acquired at the beginning of the test, serving as the undeformed reference, and the second showing the specimen condition immediately after rupture. These two frames were used as the basis for DIC analysis. From this baseline, full-field axial strain maps (ε_{xx}) were computed at selected load levels, as shown in **Figure 45**. These maps illustrate the progressive accumulation of strain in the gauge section, transitioning from a uniform axial profile to pronounced localization near the failure region. The final valid frame, captured just before rupture, marked the limit of usable data. Although the system could not capture the exact moment of fracture, due to the abrupt failure and limited field of view, the data were sufficient to characterize the evolution of strain leading up to failure.

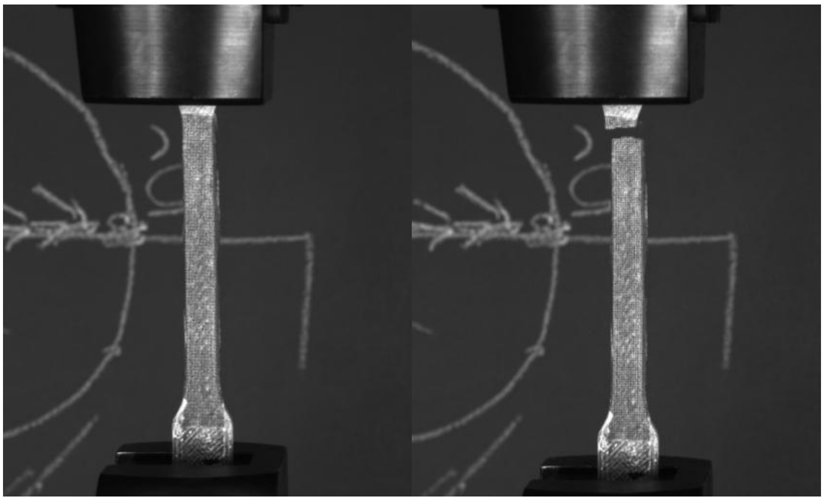

Figure 44. *Reference images used in DIC: initial undeformed state (left) and post-failure condition (right).*

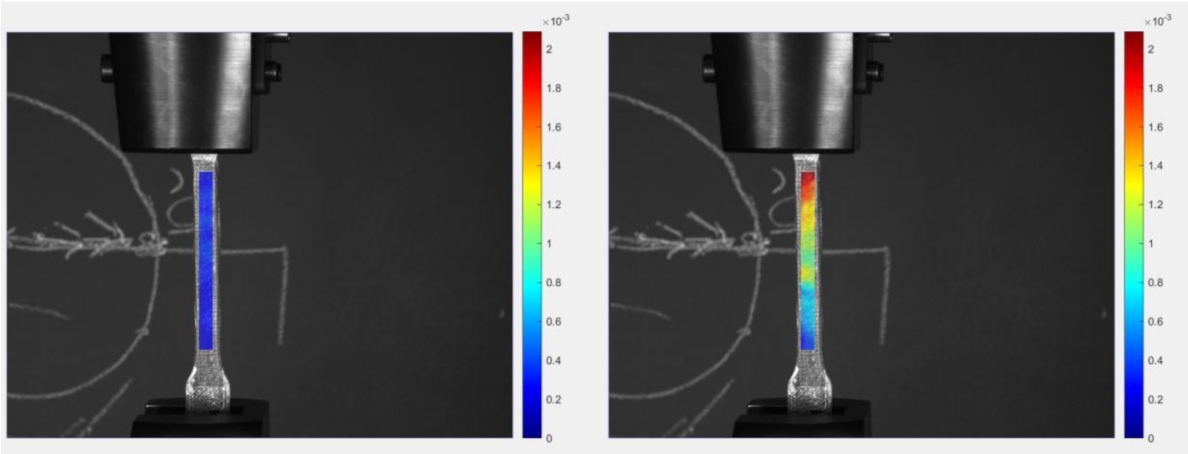

Figure 45. *Axial strain (ε_{xx}) maps obtained via DIC during loading, showing the reference image before the test begins (left) and strain localization before rupture (right).*

Although one of the original objectives of implementing DIC was to compare experimental full-field strain maps to numerical distributions obtained from the FEA simulation, this correlation could not be meaningfully carried out. The ε_{xx} fields recorded were limited to early elastic deformation and did not encompass failure progression or boundary conditions comparable to the simulation model. Nonetheless, the technique demonstrated its utility for qualitative strain assessment and, with further optimization, holds promise for more robust experimental-numerical comparisons in future studies.

In summary, DIC provided valuable insight into early-stage deformation behavior in FFF-printed PLA, despite the challenges associated with full-field acquisition and failure tracking. The method demonstrated clear potential for non-contact, spatially resolved strain analysis, particularly in capturing deformation heterogeneity that may not be detected by point-based extensometer. However, the findings also highlight the importance of optimizing the optical setup, speckle pattern uniformity, and camera alignment to fully exploit DIC's capabilities in future mechanical studies involving printed polymers.

3.3.4. Numerical and Experimental Tensile Comparison

The finite element simulation was developed to replicate the mechanical behavior of PLA tensile specimens under uniaxial loading, using an idealized linear elastic, isotropic material model. Boundary conditions and specimen geometry were defined to closely match the experimental setup, ensuring meaningful comparison.

The analysis focused on total deformation, maximum principal strain, and maximum principal stress distributions. As illustrated in **Figure 46**, **Figure 47** and **Figure 48** the results show that deformation and stress are primarily concentrated near the fillet transitions between the gauge section and the gripping ends, areas prone to localized amplification due to geometric discontinuities. This distribution aligns with the typical failure locations observed experimentally. In contrast, the central gauge region displays a more uniform response under uniaxial loading. The absence of abrupt gradients or numerical artifacts further indicates that the applied mesh and boundary conditions were suitable for capturing the expected elastic behavior.

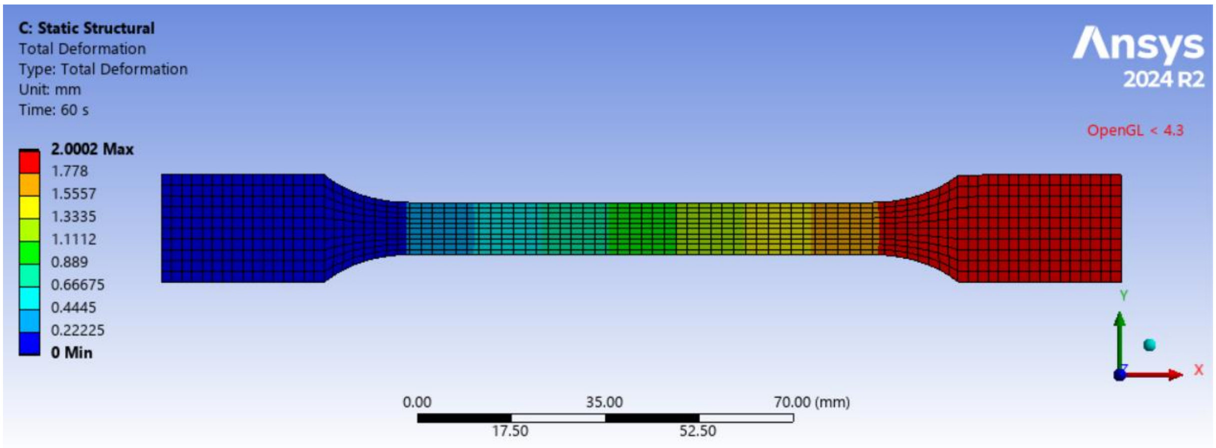

Figure 46. *Total deformation field under uniaxial tensile loading, showing displacement concentration near the transition fillets.*

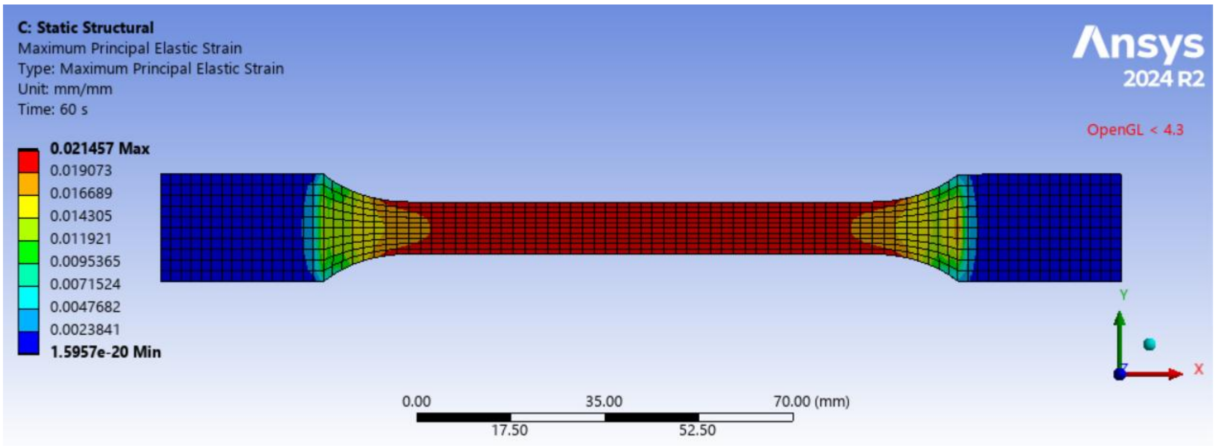

Figure 47. *Maximum principal elastic strain distribution, with localized strain amplification at the gauge-to-grip interface.*

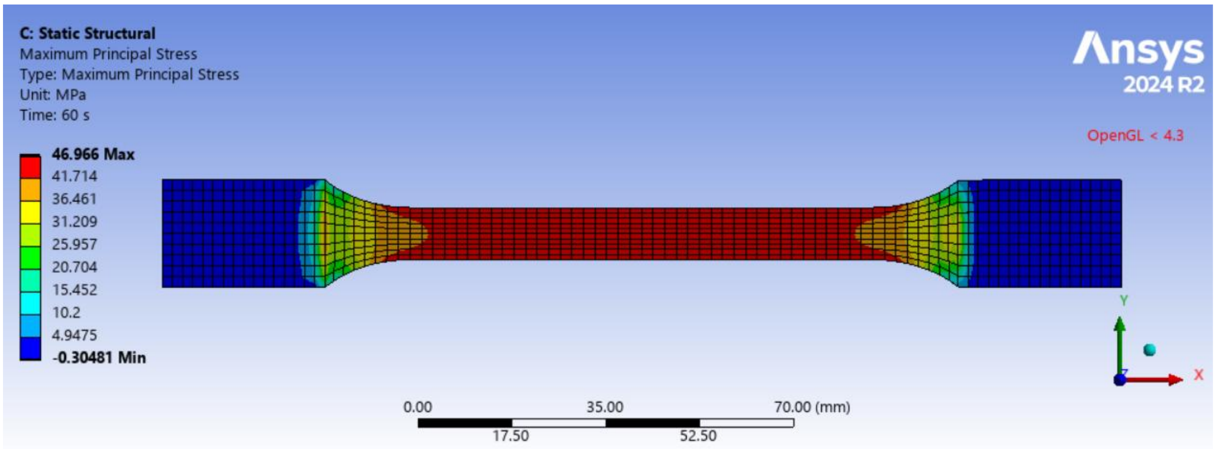

Figure 48. *Maximum principal stress distribution, highlighting stress concentration near geometric discontinuities at the specimen fillets.*

A quantitative comparison between the simulation and experiment is shown in **Figure 49**, which overlays the simulated stress-strain curve with that obtained from specimen 8, the only tested sample that presented a complete, uninterrupted response. The stress-strain curves show excellent agreement throughout the elastic region, with the numerical model closely matching the slope and initial response of the experimental data. The linear behavior assumed in the simulation was sufficient to accurately capture the material stiffness. Although the experimental curve exhibits slight nonlinearity near the peak stress, the overall correlation between the two results remains strong. This comparison confirms the model's validity for predicting the elastic performance of the printed PLA specimens under uniaxial loading.

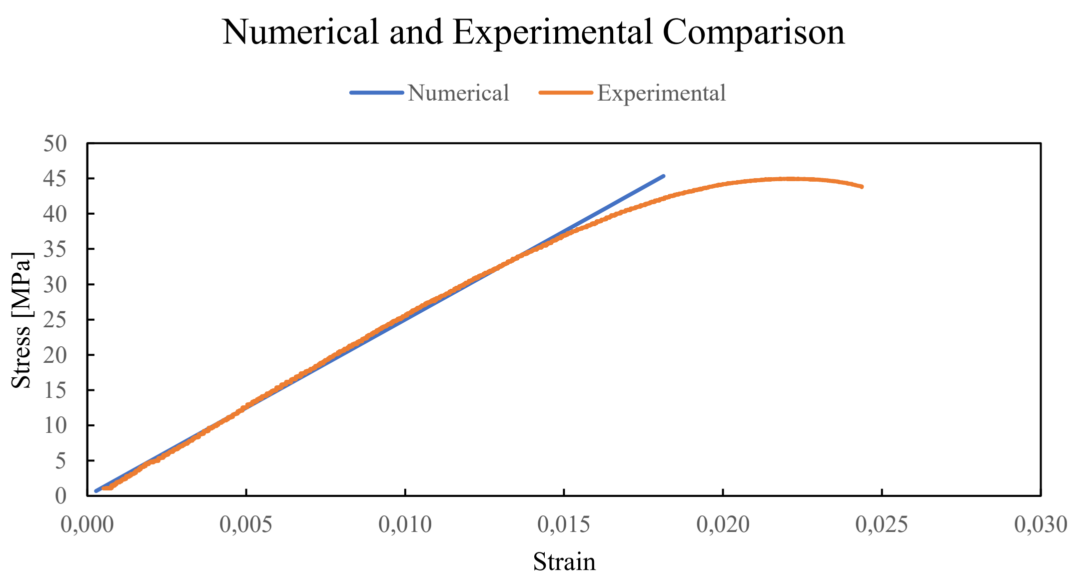

Figure 49. *Comparison between simulated and experimental stress–strain curve from specimen 8 under uniaxial loading.*

Specimen 8 fractured within the central gauge section and showed no signs of delamination or geometric asymmetry, making it an ideal candidate for simulation validation. It represented the most favorable manufacturing outcome, with minimal variation in geometry and interlayer bonding, thus offering the best experimental analog to the model assumptions. Minor discrepancies observed beyond the stress at maximum load are expected and result from the absence of plasticity, damage evolution, or cohesive failure mechanisms in the current model, which are restricted to purely elastic behavior. While this limits its applicability in capturing post-yield phenomena and failure, the model proved accurate in identifying stress concentration zones, capturing the elastic mechanical response, and predicting the global deformation trend under ideal conditions.

In summary, the simulation closely replicated the experimental behavior of the most representative specimen, confirming its validity for elastic analysis of FFF-printed PLA. These results support the use of linear finite element modeling for evaluating stiffness and stress distribution if fabrication variability and failure mechanisms are controlled or separately accounted for.

3.4. Conclusions

This study sought to evaluate the mechanical behavior of PLA specimens manufactured by FFF through experimental tensile testing and finite element simulation. The methodology was designed to ensure traceability, geometric control, and consistency between the experimental and numerical domains, following international standards for specimen design (ISO 527-1) and additive manufacturing testing.

The thermal simulation of the deposition process provided a detailed view of the transient temperature distribution in the PLA during printing, capturing the localized heating and rapid cooling that occurs after each cluster activation. The experimental thermal image confirmed the presence of similar gradients, supporting the validity of the simulation model. Although the comparison was qualitative, the good agreement between simulated and observed thermal patterns reinforces the use of the DED-based approach for evaluating heat transfer during FFF. These results establish a foundational step toward the analysis of thermally induced residual stresses, which will be addressed in future studies.

The use of DVE enabled precise acquisition of axial strain data across the gauge region, yielding reliable measurements of elastic modulus, tensile strength, and strain at rupture. However, the test results also revealed key limitations related to the brittleness of PLA. Several specimens exhibited premature fracture at transition zones, and microscopic analysis confirmed the presence of interlayer delamination and internal voids, defects intrinsic to the FFF process that significantly impacted the mechanical response.

In the DIC-based testing group, efforts to capture full-field strain data were partially successful. Although the optical setup was optimized and synchronization between load and image acquisition was achieved, several technical challenges compromised the effectiveness of this technique. Most notably, fracture often occurred outside the camera's field of view, while loss of speckle contrast and out-of-plane displacements further hindered correlation tracking. As a result, only partial strain data from the elastic regime could be recovered. These measurements nonetheless proved useful, exhibiting lower variability in elastic modulus compared to the DVE group. This improvement was attributed to the prior calibration of the printer's Z-axis, which enhanced dimensional accuracy and helped standardize specimen thickness around the nominal value of 4 mm.

The FEA analysis successfully reproduced the stress and strain distributions expected for a PLA tensile specimen under ideal loading. The model incorporated isotropic linear elastic behavior and was validated against experimental results from specimen 8, the only sample to undergo complete failure in the gauge region without significant geometric or structural defects. The comparison showed good agreement in the elastic regime between the simulated and experimental stress-strain curves. The mesh convergence study and boundary condition design were effective in capturing the uniform deformation along the gauge section and the stress concentrations at the transition fillets.

Despite these strengths, the study also encountered critical challenges that must be addressed in future work. The inconsistency in specimen quality, linked to filament variability, extrusion calibration, and print bed leveling, resulted in irregular cross-sectional areas and unexpected failure locations. Moreover, the full potential of DIC could not be realized due to limitations in ROI framing, fracture predictability, and speckle pattern durability. Addressing these issues would involve improved print parameter control, more robust speckle application methods, and enhanced alignment between the mechanical setup and optical system. Additionally, the use of high-speed cameras or stereo-DIC could improve strain tracking at rupture.

In addition, although ISO 527-1 provides a standardized framework for testing polymeric materials, it remains broad in its specifications and tolerances. In the context of FFF-printed PLA, this flexibility allowed considerable geometric and mechanical variability to arise between specimens, even when all nominal requirements were met. This finding suggests that, for additively manufactured brittle materials, stricter controls and supplementary quality checks may be necessary to ensure reproducible testing outcomes.

In conclusion, the integration of experimental testing, digital strain measurement, and numerical modeling proved effective for characterizing the tensile behavior of FFF-printed PLA. When print quality is tightly controlled and optical methods are properly configured, linear elastic models can capture the mechanical response with a high degree of fidelity. Although a full-field comparison between DIC and simulation was not achieved, the study established a methodological framework and identified key parameters that influence data quality and model reliability. These findings not only validate the feasibility of combining experimental and computational approaches in polymer mechanics but also provide a basis for improving specimen preparation, optical tracking, and simulation accuracy in future research involving additively manufactured materials.

Chapter 4

4.1. Global Conclusions and Future Directions

This work combined simulation and experimental testing to investigate the mechanical behavior of PLA parts produced by FFF. Finite element modeling was central to the approach, allowing both the thermal conditions during deposition and the mechanical response under tensile loading to be analyzed in a controlled and repeatable way. The structural simulation successfully captured the elastic behavior of printed specimens, and the thermal simulation reproduced the temperature evolution during layer deposition, helping to contextualize the process conditions that lead to mechanical variation.

From the experimental side, the study revealed how even small variations in printing parameters, such as Z-axis calibration, extrusion overlap, or inconsistent bonding between layers, can significantly affect part performance. Defects like premature fracture, interlayer delamination, and dimensional deviations were observed in several specimens, despite adherence to standardized geometry and testing protocols. These findings underscore the sensitivity of PLA to processing conditions, indicating that, in many cases, process control has a greater influence on material performance than adherence to nominal standards.

More importantly, these experimental results had a direct impact on the direction of the NaturFAB project. The inconsistencies observed led to the recognition that process interference could be a major variable in the mechanical performance of printed parts. As a result, new investigations were initiated within the project to study how specific fabrication parameters influence structural integrity. The data generated in this thesis played a key role in motivating that shift and provided a baseline for controlled experimentation going forward.

To support this next phase, the simulation framework developed here will be expanded to include residual stress analysis. Using the thermal history already simulated, it will be possible to model how internal stresses form during the printing process and how they may contribute to failure mechanisms or geometric instability. These predictions will be tested experimentally, comparing parts printed under both nominal and interfered conditions, to identify the relationship between thermal input, stress development, and mechanical reliability.

Together, these efforts will improve our understanding of how process, structure, and performance are connected in additive manufacturing. The methodology outlined in this work, linking simulation, experimental validation, and parameter tracking, sets the stage for more advanced studies, including nonlinear behavior, failure analysis, and the extension to fiber-reinforced PLA. It also directly contributes to NaturFAB broader goal of developing robust, sustainable, and locally adaptable additive manufacturing strategies.

References

[1] I. Gibson, D. Rosen, and B. Stucker, *Additive Manufacturing Technologies*. New York, NY: Springer New York, 2015. doi: 10.1007/978-1-4939-2113-3.

[2] S. Behseresht, Y. H. Park, A. Love, and O. A. Valdez Pastrana, "Application of Numerical Modeling and Finite Element Analysis in Fused Filament Fabrication: A Review," *Materials*, vol. 17, no. 17, p. 4185, Aug. 2024, doi: 10.3390/ma17174185.

[3] M. Rodríguez-Martín, R. Domingo, and J. Ribeiro, "Mapping and prospective of additive manufacturing in the context of Industry 4.0 and 5.0," *Rapid Prototyp J*, vol. 30, no. 7, pp. 1393–1410, Jul. 2024, doi: 10.1108/RPJ-11-2023-0410.

[4] N. T. Tuli, S. Khatun, and A. Bin Rashid, "Unlocking the future of precision manufacturing: A comprehensive exploration of 3D printing with fiber-reinforced composites in aerospace, automotive, medical, and consumer industries," *Heliyon*, vol. 10, no. 5, p. e27328, Mar. 2024, doi: 10.1016/j.heliyon.2024.e27328.

[5] Z. Wang and D. E. Smith, "Finite element modelling of fully-coupled flow/fiber-orientation effects in polymer composite deposition additive manufacturing nozzle-extrudate flow," *Compos B Eng*, vol. 219, p. 108811, Aug. 2021, doi: 10.1016/j.compositesb.2021.108811.

[6] C. Abhishek and N. Raghukiran, "Residual stresses in 4D printed structures: A review on causes, effects, measurements, mitigations and its applications," *Forces in Mechanics*, vol. 18, p. 100304, Feb. 2025, doi: 10.1016/j.finmec.2024.100304.

[7] E. García Plaza, P. Núñez López, M. Caminero Torija, and J. Chacón Muñoz, "Analysis of PLA Geometric Properties Processed by FFF Additive Manufacturing: Effects of Process Parameters and Plate-Extruder Precision Motion," *Polymers (Basel)*, vol. 11, no. 10, p. 1581, Sep. 2019, doi: 10.3390/polym11101581.

[8] X. Xu, H. Ren, S. Chen, X. Luo, F. Zhao, and Y. Xiong, "Review on melt flow simulations for thermoplastics and their fiber reinforced composites in fused deposition modeling," *J Manuf Process*, vol. 92, pp. 272–286, Apr. 2023, doi: 10.1016/j.jmapro.2023.02.039.

[9] S. F. Costa, F. M. Duarte, and J. A. Covas, "Thermal conditions affecting heat transfer in FDM/FFE: a contribution towards the numerical modelling of the process," *Virtual Phys Prototyp*, vol. 10, no. 1, pp. 35–46, Jan. 2015, doi: 10.1080/17452759.2014.984042.

[10] S. Dai, K. Zhu, S. Wang, and Z. Deng, "Additively manufactured materials: A critical review on their anisotropic mechanical properties and modeling methods," *J Manuf Process*, vol. 141, pp. 789–814, May 2025, doi: 10.1016/j.jmapro.2025.02.038.

[11] A. El Moumen, M. Tarfaoui, and K. Lafdi, "Modelling of the temperature and residual stress fields during 3D printing of polymer composites," *The International Journal of Advanced Manufacturing Technology*, vol. 104, no. 5–8, pp. 1661–1676, Oct. 2019, doi: 10.1007/s00170-019-03965-y.

[12] J. Wang and P. Papadopoulos, "Coupled thermomechanical analysis of fused deposition using the finite element method," *Finite Elements in Analysis and Design*, vol. 197, p. 103607, Dec. 2021, doi: 10.1016/j.finel.2021.103607.

[13] A. Al Rashid and M. Koç, "Fused Filament Fabrication Process: A Review of Numerical Simulation Techniques," *Polymers (Basel)*, vol. 13, no. 20, p. 3534, Oct. 2021, doi: 10.3390/polym13203534.

[14] A. Cattenone, S. Morganti, G. Alaimo, and F. Auricchio, "Finite Element Analysis of Additive Manufacturing Based on Fused Deposition Modeling: Distortions Prediction and Comparison With Experimental Data," *J Manuf Sci Eng*, vol. 141, no. 1, Jan. 2019, doi: 10.1115/1.4041626.

[15] M. Domingo-Espin, J. M. Puigoriol-Forcada, A.-A. Garcia-Granada, J. Llumà, S. Borros, and G. Reyes, "Mechanical property characterization and simulation of fused deposition modeling Polycarbonate parts," *Mater Des*, vol. 83, pp. 670–677, Oct. 2015, doi: 10.1016/j.matdes.2015.06.074.

[16] M. Zouaoui, J. Gardan, P. Lafon, A. Makke, C. Labergere, and N. Recho, "A Finite Element Method to Predict the Mechanical Behavior of a Pre-Structured Material Manufactured by Fused Filament Fabrication in 3D Printing," *Applied Sciences*, vol. 11, no. 11, p. 5075, May 2021, doi: 10.3390/app11115075.

[17] S. Tabacu and C. Ducu, "Numerical investigations of 3D printed structures under compressive loads using damage and fracture criterion: Experiments, parameter identification, and validation," *Extreme Mech Lett*, vol. 39, Sep. 2020, doi: 10.1016/j.eml.2020.100775.

[18] N. Maqsood, M. Rimašauskas, M. Ghobakhloo, G. Mordas, and K. Skotnicová, "Additive manufacturing of continuous carbon fiber reinforced polymer composites using materials extrusion process. Mechanical properties, process parameters, fracture analysis, challenges, and future prospect. A review," *Adv Compos Hybrid Mater*, vol. 7, no. 6, p. 202, Dec. 2024, doi: 10.1007/s42114-024-01035-w.

[19] Z. Zhang, C. Hu, and Q.-H. Qin, "The improvement of void and interface characteristics in fused filament fabrication-based polymers and continuous carbon fiber-reinforced polymer composites: a comprehensive review," *The International Journal of Advanced Manufacturing Technology*, vol. 137, no. 3–4, pp. 1047–1087, Mar. 2025, doi: 10.1007/s00170-025-15240-4.

[20] Z. Jin, Z. Zhang, and G. X. Gu, "Automated Real-Time Detection and Prediction of Interlayer Imperfections in Additive Manufacturing Processes Using Artificial Intelligence," *Advanced Intelligent Systems*, vol. 2, no. 1, Jan. 2020, doi: 10.1002/aisy.201900130.

[21] Y. Fu, A. R. J. Downey, L. Yuan, H.-T. Huang, and E. A. Ogunniyi, "Simulation-in-the-loop additive manufacturing for real-time structural validation and digital twin development," *Addit Manuf*, vol. 98, p. 104631, Jan. 2025, doi: 10.1016/j.addma.2024.104631.

[22] L. Lu, J. Hou, S. Yuan, X. Yao, Y. Li, and J. Zhu, "Deep learning-assisted real-time defect detection and closed-loop adjustment for additive manufacturing of continuous fiber-reinforced polymer composites," *Robot Comput Integr Manuf*, vol. 79, p. 102431, Feb. 2023, doi: 10.1016/j.rcim.2022.102431.

[23] A. Morvayová, N. Contuzzi, and G. Casalino, "Defects and residual stresses finite element prediction of FDM 3D printed wood/PLA biocomposite," *The International Journal of Advanced Manufacturing Technology*, vol. 129, no. 5–6, pp. 2281–2293, Nov. 2023, doi: 10.1007/s00170-023-12410-0.

[24] M. R. Khosravani, S. Rezaei, H. Ruan, and T. Reinicke, "Fracture behavior of anisotropic 3D-printed parts: experiments and numerical simulations," *Journal of Materials Research and Technology*, vol. 19, pp. 1260–1270, Jul. 2022, doi: 10.1016/j.jmrt.2022.05.068.

[25] A. Garg and A. Bhattacharya, "An insight to the failure of FDM parts under tensile loading: finite element analysis and experimental study," *Int J Mech Sci*, vol. 120, pp. 225–236, Jan. 2017, doi: 10.1016/j.ijmecsci.2016.11.032.

[26] Z. Yang, Z. Yang, H. Chen, and W. Yan, “3D printing of short fiber reinforced composites via material extrusion: Fiber breakage,” *Addit Manuf*, vol. 58, p. 103067, Oct. 2022, doi: 10.1016/j.addma.2022.103067.

[27] T. Yap, Z. He, Z. Wang, A. Tamijani, and M. Tehrani, “Experimental investigation and validation of strength-based topology and fiber path optimization in additively manufactured continuous fiber reinforced composites,” *Addit Manuf*, vol. 89, p. 104274, Jun. 2024, doi: 10.1016/j.addma.2024.104274.

[28] B. P. Heller, D. E. Smith, and D. A. Jack, “Planar deposition flow modeling of fiber filled composites in large area additive manufacturing,” *Addit Manuf*, vol. 25, pp. 227–238, Jan. 2019, doi: 10.1016/j.addma.2018.10.031.

[29] A. Awenlimobor, D. E. Smith, and Z. Wang, “Simulation of fiber-induced melt pressure fluctuations within large scale polymer composite deposition beads,” *Addit Manuf*, vol. 80, p. 103980, Jan. 2024, doi: 10.1016/j.addma.2024.103980.

[30] J. Ribeiro *et al.*, “New trends of additive manufacturing using materials based-on natural fibers and minerals : A systematic review,” *Heliyon*, vol. 11, no. 2, p. e41993, Jan. 2025, doi: 10.1016/j.heliyon.2025.e41993.

[31] M. Rodríguez-Martín *et al.*, “Predictive Models for the Characterization of Internal Defects in Additive Materials from Active Thermography Sequences Supported by Machine Learning Methods,” *Sensors*, vol. 20, no. 14, p. 3982, Jul. 2020, doi: 10.3390/s20143982.

[32] M. Rodríguez-Martín *et al.*, “Step heating thermography supported by machine learning and simulation for internal defect size measurement in additive manufacturing,” *Measurement*, vol. 205, p. 112140, Dec. 2022, doi: 10.1016/j.measurement.2022.112140.

[33] I. Zupic and T. Čater, “Bibliometric Methods in Management and Organization,” *Organ Res Methods*, vol. 18, no. 3, pp. 429–472, Jul. 2015, doi: 10.1177/1094428114562629.

[34] S. C. Altıparmak, V. A. Yardley, Z. Shi, and J. Lin, “Extrusion-based additive manufacturing technologies: State of the art and future perspectives,” *J Manuf Process*, vol. 83, pp. 607–636, Nov. 2022, doi: 10.1016/j.jmapro.2022.09.032.

[35] S. Jaganathan, R. Kandasamy, R. Venkatachalam, M. Gunalan, and R. Dhairiyasamy, “Advances in Optimizing Mechanical Performance of 3D-Printed Polymer Composites: A Microstructural and Processing Enhancements Review,” *Advances in Polymer Technology*, vol. 2024, no. 1, Jan. 2024, doi: 10.1155/2024/3168252.

[36] Y. Tao *et al.*, “A review on voids of 3D printed parts by fused filament fabrication,” *Journal of Materials Research and Technology*, vol. 15, pp. 4860–4879, Nov. 2021, doi: 10.1016/j.jmrt.2021.10.108.

[37] G. Chen *et al.*, “Regulated the orientation of graphene nanoplatelets via flow field in material extrusion for enhancing thermal conductivity,” *Addit Manuf*, vol. 101, p. 104718, Mar. 2025, doi: 10.1016/j.addma.2025.104718.

[38] A. Das, J. A. Riet, M. J. Bortner, and C. McIlroy, “Rheology, crystallization, and process conditions: The effect on interlayer properties in three-dimensional printing,” *Physics of Fluids*, vol. 34, no. 12, Dec. 2022, doi: 10.1063/5.0128660.

[39] C. Iandiorio, G. Mattei, E. Marotta, G. Costanza, M. E. Tata, and P. Salvini, “The Beneficial Effect of a TPMS-Based Fillet Shape on the Mechanical Strength of Metal Cubic Lattice Structures,” *Materials*, vol. 17, no. 7, p. 1553, Mar. 2024, doi: 10.3390/ma17071553.

[40] A. Ceci, C. Cerini, G. Costanza, and M. E. Tata, "Production of Al Alloys with Kelvin Cells Using the Lost-PLA Technique and Their Mechanical Characterization via Compression Tests," *Materials*, vol. 18, no. 2, p. 296, Jan. 2025, doi: 10.3390/ma18020296.

[41] M. K. Agarwala, V. R. Jamalabad, N. A. Langrana, A. Safari, P. J. Whalen, and S. C. Danforth, "Structural quality of parts processed by fused deposition," *Rapid Prototyp J*, vol. 2, no. 4, pp. 4–19, Dec. 1996, doi: 10.1108/13552549610732034.

[42] N. Venkataraman *et al.*, "Feedstock material property – process relationships in fused deposition of ceramics (FDC)," *Rapid Prototyp J*, vol. 6, no. 4, pp. 244–253, Dec. 2000, doi: 10.1108/13552540010373344.

[43] B. N. Turner, R. Strong, and S. A. Gold, "A review of melt extrusion additive manufacturing processes: I. Process design and modeling," *Rapid Prototyp J*, vol. 20, no. 3, pp. 192–204, Apr. 2014, doi: 10.1108/RPJ-01-2013-0012.

[44] G. Schramm, *A Practical Approach to Rheology and Rheometry*. Karlsruhe: Haake, 1994.

[45] S. Manrich, *Processamento de Termoplásticos: Rosca Única, Extrusão e Matrizes, Injeção e Moldes*. São Paulo: Artliber Editora, 2005.

[46] D. D. Phan, J. S. Horner, Z. R. Swain, A. N. Beris, and M. E. Mackay, "Computational fluid dynamics simulation of the melting process in the fused filament fabrication additive manufacturing technique," *Addit Manuf*, vol. 33, p. 101161, May 2020, doi: 10.1016/j.addma.2020.101161.

[47] N. P. Cheremisinoff, *An Introduction to Polymer Rheology and Processing*. Boca Raton: CRC Press, 1993.

[48] R. E. S. Bretas and M. A. D'Ávila, *Reologia de Polímeros Fundidos*. São Carlos: EdUFSCar, 2000.

[49] R. J. Poole, "Inelastic and flow-type parameter models for non-Newtonian fluids," *J Nonnewton Fluid Mech*, vol. 320, p. 105106, Oct. 2023, doi: 10.1016/j.jnnfm.2023.105106.

[50] D. V. Rosato, *Rosato's Plastics Encyclopedia and Dictionary*. Munich: Hanser Publishers, 1993.

[51] J. A. Bradson, *Flow Properties of Polymer Melts*, 2nd ed. London: George Godwin Ltd., 1981.

[52] C. Rauwendaal, *Polymer Extrusion*. New York: Hanser Publishers, 1990.

[53] C. Yang, X. Tian, D. Li, Y. Cao, F. Zhao, and C. Shi, "Influence of thermal processing conditions in 3D printing on the crystallinity and mechanical properties of PEEK material," *J Mater Process Technol*, vol. 248, pp. 1–7, Oct. 2017, doi: 10.1016/j.jmatprotec.2017.04.027.

[54] R. Comminal, M. P. Serdeczny, D. B. Pedersen, and J. Spangenberg, "Numerical modeling of the strand deposition flow in extrusion-based additive manufacturing," *Addit Manuf*, vol. 20, pp. 68–76, Mar. 2018, doi: 10.1016/j.addma.2017.12.013.

[55] M. P. Serdeczny, R. Comminal, Md. T. Mollah, D. B. Pedersen, and J. Spangenberg, "Viscoelastic simulation and optimisation of the polymer flow through the hot-end during filament-based material extrusion additive manufacturing," *Virtual Phys Prototyp*, vol. 17, no. 2, pp. 205–219, Apr. 2022, doi: 10.1080/17452759.2022.2028522.

[56] M. P. Serdeczny, R. Comminal, Md. T. Mollah, D. B. Pedersen, and J. Spangenberg, "Numerical modeling of the polymer flow through the hot-end in filament-based material extrusion additive manufacturing," *Addit Manuf*, vol. 36, p. 101454, Dec. 2020, doi: 10.1016/j.addma.2020.101454.

[57] D.-I. Jeong, A. Jain, and D.-W. Oh, "Increasing perpendicular alignment in extruded filament by an orifice embedded 3D printing nozzle," *Virtual Phys Prototyp*, vol. 17, no. 1, pp. 1–18, Jan. 2022, doi: 10.1080/17452759.2021.1980935.

[58] T. Schuller, M. Jalaal, P. Fanzio, and F. J. Galindo-Rosales, "Optimal shape design of printing nozzles for extrusion-based additive manufacturing," *Addit Manuf*, vol. 84, p. 104130, Mar. 2024, doi: 10.1016/j.addma.2024.104130.

[59] S. Liparoti, D. Sofia, A. Romano, F. Marra, and R. Pantani, "Fused Filament Deposition of PLA: The Role of Interlayer Adhesion in the Mechanical Performances," *Polymers (Basel)*, vol. 13, no. 3, p. 399, Jan. 2021, doi: 10.3390/polym13030399.

[60] J. Zhang, X. Z. Wang, W. W. Yu, and Y. H. Deng, "Numerical investigation of the influence of process conditions on the temperature variation in fused deposition modeling," *Mater Des*, vol. 130, pp. 59–68, Sep. 2017, doi: 10.1016/j.matdes.2017.05.040.

[61] Y. Zhou, T. Nyberg, G. Xiong, and D. Liu, "Temperature Analysis in the Fused Deposition Modeling Process," in *2016 3rd International Conference on Information Science and Control Engineering (ICISCE)*, IEEE, Jul. 2016, pp. 678–682. doi: 10.1109/ICISCE.2016.150.

[62] T. J. Coogan and D. O. Kazmer, "Healing simulation for bond strength prediction of FDM," *Rapid Prototyp J*, vol. 23, no. 3, pp. 551–561, Apr. 2017, doi: 10.1108/RPJ-03-2016-0051.

[63] A. Lepoivre, N. Boyard, A. Levy, and V. Sobotka, "Heat Transfer and Adhesion Study for the FFF Additive Manufacturing Process," *Procedia Manuf*, vol. 47, pp. 948–955, 2020, doi: 10.1016/j.promfg.2020.04.291.

[64] J. Go, S. N. Schiffres, A. G. Stevens, and A. J. Hart, "Rate limits of additive manufacturing by fused filament fabrication and guidelines for high-throughput system design," *Addit Manuf*, vol. 16, pp. 1–11, Aug. 2017, doi: 10.1016/j.addma.2017.03.007.

[65] H. Xia, J. Lu, and G. Tryggvason, "Fully resolved numerical simulations of fused deposition modeling. Part II – solidification, residual stresses and modeling of the nozzle," *Rapid Prototyp J*, vol. 24, no. 6, pp. 973–987, Oct. 2018, doi: 10.1108/RPJ-11-2017-0233.

[66] M. P. Serdeczny, "Numerical and Experimental Analysis of Filament-based Material Extrusion Additive Manufacturing," Technical University of Denmark, Denmark, 2020.

[67] T.-M. Wang, J.-T. Xi, and Y. Jin, "A model research for prototype warp deformation in the FDM process," *The International Journal of Advanced Manufacturing Technology*, vol. 33, no. 11–12, pp. 1087–1096, Aug. 2007, doi: 10.1007/s00170-006-0556-9.

[68] S. Bhandari and R. A. Lopez-Anido, "Discrete-Event Simulation Thermal Model for Extrusion-Based Additive Manufacturing of PLA and ABS," *Materials*, vol. 13, no. 21, p. 4985, Nov. 2020, doi: 10.3390/ma13214985.

[69] B. Jiang, "Thermal simulations for guiding 3D printed polymers and composites used in Fused Filament Fabrication.," Thesis, The University of Sydney, Sydney, 2023.

[70] D. Croccolo, M. De Agostinis, and G. Olmi, "Experimental characterization and analytical modelling of the mechanical behaviour of fused deposition processed parts made of ABS-M30," *Comput Mater Sci*, vol. 79, pp. 506–518, Nov. 2013, doi: 10.1016/j.commatsci.2013.06.041.

[71] M. Kohutiar *et al.*, "Study of selected thermoplastics using dynamic mechanical analysis," *MATEC Web of Conferences*, vol. 157, p. 07002, Mar. 2018, doi: 10.1051/matecconf/201815707002.

[72] M. Wikło, B. H. Byczuk, and K. Skrzek, "Mechanical Characterization of FDM 3D-Printed Components Using Advanced Measurement and Modeling Techniques," *Materials*, vol. 18, no. 5, p. 1086, Feb. 2025, doi: 10.3390/ma18051086.

[73] H. L. Tekinalp *et al.*, "Highly oriented carbon fiber–polymer composites via additive manufacturing," *Compos Sci Technol*, vol. 105, pp. 144–150, Dec. 2014, doi: 10.1016/j.compscitech.2014.10.009.

[74] B. Brenken, E. Barocio, A. Favaloro, V. Kunc, and R. B. Pipes, "Fused filament fabrication of fiber-reinforced polymers: A review," *Addit Manuf*, vol. 21, pp. 1–16, May 2018, doi: 10.1016/j.addma.2018.01.002.

[75] D. Yang, K. Wu, L. Wan, and Y. Sheng, "A Particle Element Approach for Modelling the 3D Printing Process of Fibre Reinforced Polymer Composites," *Journal of Manufacturing and Materials Processing*, vol. 1, no. 1, p. 10, Sep. 2017, doi: 10.3390/jmmp1010010.

[76] Z. Yang, K. Fu, Z. Zhang, J. Zhang, and Y. Li, "Topology optimization of 3D-printed continuous fiber-reinforced composites considering manufacturability," *Compos Sci Technol*, vol. 230, p. 109727, Nov. 2022, doi: 10.1016/j.compscitech.2022.109727.

[77] B. Brenken, E. Barocio, A. Favaloro, V. Kunc, and R. B. Pipes, "Development and validation of extrusion deposition additive manufacturing process simulations," *Addit Manuf*, vol. 25, pp. 218–226, Jan. 2019, doi: 10.1016/j.addma.2018.10.041.

[78] I. Plamadiala, C. Croitoru, M. A. Pop, and I. C. Roata, "Enhancing Polylactic Acid (PLA) Performance: A Review of Additives in Fused Deposition Modelling (FDM) Filaments," *Polymers (Basel)*, vol. 17, no. 2, p. 191, Jan. 2025, doi: 10.3390/polym17020191.

[79] M. Somireddy, A. Czekanski, and S. V. Atre, "Modelling of Failure Behaviour of 3D-Printed Composite Parts," *Applied Sciences*, vol. 12, no. 21, p. 10724, Oct. 2022, doi: 10.3390/app122110724.

[80] S. Ouyang *et al.*, "Process modeling and deformation prediction of 3D printed continuous fiber-reinforced composites based on in-situ micro-scale measuring," *Compos Sci Technol*, vol. 267, p. 111209, Jul. 2025, doi: 10.1016/j.compscitech.2025.111209.

[81] E. Ghane, "Learning from Data and Physics for Multiscale Modeling of Woven Composites," Doctoral Thesis, Univeristy of Gothenburg, 2025.

[82] A. Antony Samy, A. Golbang, E. Harkin-Jones, E. Archer, and A. McIlhagger, "Prediction of part distortion in Fused Deposition Modelling (FDM) of semi-crystalline polymers via COMSOL: Effect of printing conditions," *CIRP J Manuf Sci Technol*, vol. 33, pp. 443–453, May 2021, doi: 10.1016/j.cirpj.2021.04.012.

[83] Q. Xia, G. Sun, J. Kim, and Y. Li, "Multi-scale modeling and simulation of additive manufacturing based on fused deposition technique," *Physics of Fluids*, vol. 35, no. 3, Mar. 2023, doi: 10.1063/5.0141316.

[84] H. Yang and S. Zhang, "Numerical simulation of temperature field and stress field in fused deposition modeling," *Journal of Mechanical Science and Technology*, vol. 32, no. 7, pp. 3337–3344, Jul. 2018, doi: 10.1007/s12206-018-0636-4.

[85] A. Favaloro, B. Brenken, E. Barocio, and B. Pipes, "Simulation of Polymeric Composites Additive Manufacturing Using Abaqus," in *Dassault Systèmes' Science in the Age of Experience*, Chicago, 2017, pp. 103–114.

[86] B. Brenken, E. Barocio, A. J. Favaloro, and B. R. Pipes, "Simulation of Semi-Crystalline Composites in the Extrusion Deposition Additive Manufacturing Process," in *Science in the Age of Experience*, 2017, pp. 90–102.

[87] F. Talagani *et al.*, "Numerical Simulation of Big Area Additive Manufacturing (3D Printing) of a Full Size Car," SAMPE Journal, 2015.

[88] M. R. Karamooz Ravari, M. Kadkhodaei, M. Badrossamay, and R. Rezaei, "Numerical investigation on mechanical properties of cellular lattice structures fabricated by fused deposition modeling," *Int J Mech Sci*, vol. 88, pp. 154–161, Nov. 2014, doi: 10.1016/j.ijmecsci.2014.08.009.

[89] A. Alafaghani, A. Qattawi, B. Alrawi, and A. Guzman, "Experimental Optimization of Fused Deposition Modelling Processing Parameters: A Design-for-Manufacturing Approach," *Procedia Manuf*, vol. 10, pp. 791–803, 2017, doi: 10.1016/j.promfg.2017.07.079.

[90] F. Aldosari, M. A. A. Khan, M. Asad, and F. Djavanroodi, "Finite Element Analysis of PolyLactic Acid (PLA) under Tensile and Compressive Loading," *J Phys Conf Ser*, vol. 2468, no. 1, p. 012094, Apr. 2023, doi: 10.1088/1742-6596/2468/1/012094.

[91] T. Hachimi, F. Majid, N. Zekriti, R. Rhanim, and H. Rhanim, "Improvement of 3D printing polymer simulations considering converting G-code to Abaqus," *The International Journal of Advanced Manufacturing Technology*, vol. 131, no. 9–10, pp. 5193–5208, Apr. 2024, doi: 10.1007/s00170-024-13300-9.

[92] A. A. F. Ogaili *et al.*, "The Effect of Chopped Carbon Fibers on the Mechanical Properties and Fracture Toughness of 3D-Printed PLA Parts: An Experimental and Simulation Study," *Journal of Composites Science*, vol. 8, no. 7, p. 273, Jul. 2024, doi: 10.3390/jcs8070273.

[93] S. Z. Gebrehiwot, L. Espinosa Leal, J. N. Eickhoff, and L. Rechenberg, "The influence of stiffener geometry on flexural properties of 3D printed polylactic acid (PLA) beams," *Progress in Additive Manufacturing*, vol. 6, no. 1, pp. 71–81, Feb. 2021, doi: 10.1007/s40964-020-00146-2.

[94] D. B. Perez, E. Celik, and R. L. Karkkainen, "Investigation of Interlayer Interface Strength and Print Morphology Effects in Fused Deposition Modeling 3D-Printed PLA," *3D Print Addit Manuf*, vol. 8, no. 1, pp. 23–32, Feb. 2021, doi: 10.1089/3dp.2020.0109.

[95] Y. Zhang and Y. K. Chou, "Three-dimensional finite element analysis simulations of the fused deposition modelling process," *Proc Inst Mech Eng B J Eng Manuf*, vol. 220, no. 10, pp. 1663–1671, Oct. 2006, doi: 10.1243/09544054JEM572.

[96] Y. Zhang and K. Chou, "A parametric study of part distortions in fused deposition modelling using three-dimensional finite element analysis," *Proc Inst Mech Eng B J Eng Manuf*, vol. 222, no. 8, pp. 959–968, Aug. 2008, doi: 10.1243/09544054JEM990.

[97] X. Xu, W. Qiu, D. Wan, J. Wu, F. Zhao, and Y. Xiong, "Numerical modelling of the viscoelastic polymer melt flow in material extrusion additive manufacturing," *Virtual Phys Prototyp*, vol. 19, no. 1, Dec. 2024, doi: 10.1080/17452759.2023.2300666.

[98] N. A. Sukindar, M. K. A. Ariffin, B. T. H. T. Baharudin, C. N. A. Jaafar, and M. I. S. Ismail, "ANALYZING THE EFFECT OF NOZZLE DIAMETER IN FUSED DEPOSITION MODELING FOR EXTRUDING POLYLACTIC ACID USING OPEN SOURCE 3D PRINTING," *J Teknol*, vol. 78, no. 10, Sep. 2016, doi: 10.11113/jt.v78.6265.

[99] V. Harshitha and S. Srinivasa Rao, "Design and analysis of ISO standard bolt and nut in FDM 3D printer using PLA and ABS materials," *Mater Today Proc*, vol. 19, pp. 583–588, 2019, doi: 10.1016/j.matpr.2019.07.737.

[100] M. Lei, Q. Wei, M. Li, J. Zhang, R. Yang, and Y. Wang, "Numerical Simulation and Experimental Study the Effects of Process Parameters on Filament Morphology and Mechanical Properties of FDM 3D Printed PLA/GNPs Nanocomposite," *Polymers (Basel)*, vol. 14, no. 15, p. 3081, Jul. 2022, doi: 10.3390/polym14153081.

[101] B. Devender, P. Kishore Kumar, K. L. kala, and H. Vemanaboina, "Modeling and flow analysis of FDM based dual extruder," *Mater Today Proc*, Apr. 2023, doi: 10.1016/j.matpr.2023.03.794.

[102] H. Hou, Y. Yue, J. Liu, D. Xi, and S. Liu, "Numerical Simulation and Experimental Study of the Stress Formation Mechanism of FDM with Different Printing Paths," *J Renew Mater*, vol. 11, no. 1, pp. 273–289, 2023, doi: 10.32604/jrm.2023.021167.

[103] S. Ganeshkumar *et al.*, "Investigation of Tensile Properties of Different Infill Pattern Structures of 3D-Printed PLA Polymers: Analysis and Validation Using Finite Element Analysis in ANSYS," *Materials*, vol. 15, no. 15, p. 5142, Jul. 2022, doi: 10.3390/ma15155142.

[104] J. Dobos, M. M. Hanon, and I. Oldal, "Effect of infill density and pattern on the specific load capacity of FDM 3D-printed PLA multi-layer sandwich," *Journal of Polymer Engineering*, vol. 42, no. 2, pp. 118–128, Feb. 2022, doi: 10.1515/polyeng-2021-0223.

[105] C. F. Popa, T. Krausz, S.-V. Galatanu, E. Linul, and L. Marsavina, "Numerical and experimental study for FDM printed specimens from PLA under IZOD impact tests," *Mater Today Proc*, vol. 78, pp. 326–330, 2023, doi: 10.1016/j.matpr.2022.11.501.

[106] J. Li, S. Yang, D. Li, and V. Chalivendra, "Numerical and experimental studies of additively manufactured polymers for enhanced fracture properties," *Eng Fract Mech*, vol. 204, pp. 557–569, Dec. 2018, doi: 10.1016/j.engfracmech.2018.11.001.

[107] B. Banjanin *et al.*, "Consistency analysis of mechanical properties of elements produced by FDM additive manufacturing technology," *Revista Materia*, vol. 23, no. 4, 2018, doi: 10.1590/s1517-707620180004.0584.

Appendix A

List Of Publications

The development of this dissertation resulted in publications in international journals and publications in indexed journals.

Publications

Enriconi, M. et al., 2025. A Comprehensive Review of Fused Filament Fabrication: Numerical Modeling Approaches and Emerging. Applied Sciences, 15(12), 6696. https://doi.org/10.3390/app15126696.

Enriconi, M. et al., 2025. Experimental and Numerical Assessment of FFF-Printed PLA: A Comparative Study Using Optical Strain Techniques. Manuscript preparation for submission to a scientific journal.